Reward perseveration is shaped by $GABA_A$-mediated dopamine pauses

Sasha C.V. Burwell[1, 3], Haidun Yan[2, 3], Shaun S.X. Lim[2, 3], Brenda C. Shields[2, 3], and Michael R. Tadross[1, 2, 3]

[1]Department of Neurobiology, Duke University, Durham, North Carolina, USA.
[2]Department of Biomedical Engineering, Duke University, Durham, North Carolina, USA.
[3]Aligning Science Across Parkinson's (ASAP) Collaborative Research Network, Chevy Chase, Maryland, USA

correspondence: michael.tadross@duke.edu

Abstract

Extinction learning is an essential form of cognitive flexibility, which enables obsolete reward associations to be discarded. Its downregulation can lead to perseveration, a symptom seen in several neuropsychiatric disorders. This balance is regulated by dopamine from VTA_{DA} (ventral tegmental area dopamine) neurons, which in turn are largely controlled by GABA (gamma amino-butyric acid) synapses. However, the causal relationship of these circuit elements to extinction and perseveration remain incompletely understood. Here, we employ an innovative drug-targeting technology, DART (drug acutely restricted by tethering), to selectively block $GABA_A$ receptors on VTA_{DA} neurons as mice engage in Pavlovian learning. DART eliminated $GABA_A$-mediated pauses—brief decrements in VTA_{DA} activity canonically thought to drive extinction learning. However, contrary to the hypothesis that blocking VTA_{DA} pauses should eliminate extinction learning, we observed the opposite—accelerated extinction learning. Specifically, DART eliminated the naturally occurring perseveration seen in half of control mice. We saw no impact on Pavlovian conditioning, nor on other aspects of VTA_{DA} neural firing. These findings challenge canonical theories, recasting $GABA_A$-mediated VTA_{DA} pauses from presumed facilitators of extinction to drivers of perseveration. More broadly, this study showcases the merits of targeted synaptic pharmacology, while hinting at circuit interventions for pathological perseveration.

Main

To thrive, animals must learn to predict and secure rewards, such as food and water. When a predicted reward fails to materialize, individuals show variability in their responses. A moderate level of adaptability is ideal, striking a balance between persisting through occasional setbacks and adapting after repeated failure. However, excessive persistence, known as perseveration, is generally maladaptive[1-3].

By distilling reward learning to its essence, Pavlovian tasks have facilitated seminal discoveries, such as the role of VTA_{DA} neurons in calculating reward prediction error (RPE)—the difference between predicted and actual rewards[4-7]. An increase (burst) in VTA_{DA} activity signals a positive RPE, indicating an unexpected gain, while a decrease (pause) denotes a negative RPE, reflecting unmet expectations[8-11].

Beyond correlation, the RPE framework has inspired causal experiments, which have thus far delineated bursts and pauses as functionally opposing forces. Optogenetically induced VTA_{DA} bursts promote Pavlovian conditioning, the creation of new reward associations[12-21], while optogenetically induced pauses facilitate Pavlovian extinction, the dissolution of obsolete associations[22-24]. However, widefield optogenetic perturbations tend to produce synchronous events in all VTA_{DA} cells, closely resembling natural bursts where nearly all VTA_{DA} cells are recruited in unison by an external reward[25-27]. By contrast, natural VTA_{DA} pauses manifest inconsistently across cells and trials[28], reflecting the complexity of an unmet internal prediction. Thus, artificial VTA_{DA} pauses bear little resemblance to their natural counterparts.

The heterogeneity of natural pauses also complicates their elimination. On a given reward-omission trial, many VTA_{DA} neurons do not pause, while others reduce their activity to varying degrees[28]—an issue compounded by the broad range of baseline (tonic) firing rates, from 0.5 to 10 Hz[5-7]. Thus, widefield interventions cannot counteract natural VTA_{DA} pauses without producing bursts in non-pausing or weakly-pausing cells. Underscoring this concern is the sensitivity of behavior to the strength of the intervention: extinction learning is slowed by 20-Hz[14,29,30] but unaffected by 5-Hz[30] optical excitation. While single-cell, closed-loop optogenetics presents a potential solution[31,32], such precision has yet to be applied to VTA_{DA} cells.

In this study, we approach the pause-heterogeneity problem by shifting our focus from VTA_{DA} action-potential patterns to their receptor-mediated origin. Specifically, we test the hypothesis that blocking $GABA_A$ receptor-mediated pauses in VTA_{DA} cells would bias animal behavior towards perseveration. While broadly believed to be true, experimental support for this hypothesis has been indirect. VTA infusions of $GABA_A$-specific drugs[33] have been performed, as have manipulations of GABA release[34-36]. Despite their apparent support for the canonical hypothesis, these approaches impact both dopaminergic and non-dopaminergic cells in the VTA, complicating interpretation. Mice lacking the β_3 subunit of $GABA_A$ receptors, specifically in DA neurons, showed normal extinction learning; however chronic compensatory changes were seen even in non-dopaminergic cells[37]. To circumvent these issues, we focused on an innovative drug-targeting technology, DART, which offers the ability to perform cell-specific, receptor-specific manipulations that take hold within minutes[38,39].

Gabazine^{DART} is a cell-specific, $GABA_A$-specific antagonist

Our approach capitalizes on DART's ability to precisely block native $GABA_A$ receptors on VTA_{DA} neurons[39]. To achieve cellular specificity, an AAV viral vector is used to express the HTP (HaloTag Protein) exclusively on

VTA_{DA} cells of adult DAT::Cre mice. This virus expresses stably, without altering the underlying physiology of VTA_{DA} cells. At a later time of interest, we apply gabazine^{DART}, a two-headed ligand whose HTL (HaloTag Ligand) moiety is efficiently captured by HTP, while its flexible linker allows the gabazine moiety to competitively bind and antagonize native $GABA_A$ receptors (**Fig. 1a**). We co-deliver gabazine^{DART} with a small amount of Alexa647^{DART} to serve as a fluorescent proxy of drug delivery. Control mice are treated identically, except for the use of a double-dead HTP (^{dd}HTP), which cannot bind the HTL (**Fig. 1b**).

In acute brain slices, dopamine neurons expressing ^{dd}HTP were unaffected by gabazine^{DART}, whereas neurons expressing the active $^{+}$HTP exhibited a rapid and nearly complete block of $GABA_A$-mediated synaptic transmission (**Extended Data Fig. 1a**)[39]. Regarding receptor specificity, a saturating dose of tethered gabazine^{DART} did not alter AMPA or NMDA receptors, nor did it impact the intrinsic pacemaker properties or action potential waveforms of VTA_{DA} cells (**Extended Data Fig. 1b-c**). Furthermore, Alexa647^{DART} did not influence these physiological characteristics of VTA_{DA} neurons (**Extended Data Fig. 1d**). Together, these data validate that tethered gabazine^{DART} is a selective antagonist of the $GABA_A$ receptor.

Finally, prior *in-vivo* tests of safety and efficacy found no behavioral effects of ambient gabazine^{DART} when infused into the VTA of awake ^{dd}HTP mice. In $^{+}$HTP mice, tethering of gabazine^{DART} onto VTA_{DA} neurons took hold within minutes, with a single dose sufficing for two days of behavior[39].

$GABA_A$ receptors mediate VTA_{DA} pauses *in vivo*

In principle, $GABA_A$ receptors could regulate many aspects of VTA_{DA} firing[40]. We thus recorded VTA_{DA} action potentials in awake, head-fixed mice, before and after delivery of gabazine^{DART} (**Fig. 1c**). We examined a panel of tonic, burst, and pause metrics, using a sliding-window analysis spanning pre-gabazine^{DART} (15 min), drug infusion/equilibration (75 min), and post-gabazine^{DART} (15 min) periods. In ^{dd}HTP mice, all metrics remained stable throughout the recording, indicating negligible effects of ambient gabazine^{DART} (**Extended Data Fig. 2a**).

In comparing $^{+}$HTP mice to ^{dd}HTP controls, we found that gabazine^{DART} substantially reduced the occurrence of spontaneous pauses. The effect is seen most readily in the main pause metric, ***%PSI***, the percent of interspike intervals longer than twice the median interval. This metric was reduced by gabazine^{DART} in $^{+}$HTP mice relative to ^{dd}HTP controls (two-sided permutation test, P=0.009, **Fig. 1d**). The effect was robust to adjustments in the definition of a pause, and could not be explained by a symmetrical change in interspike-interval variance (**Extended Data Fig. 2b**). All other metrics exhibited no significant difference in $^{+}$HTP vs ^{dd}HTP mice (**Fig. 1e-f**, **Extended Data Fig. 2c-e**). Thus, the main effect of gabazine^{DART} is to prevent natural $GABA_A$-mediated VTA_{DA} pauses from occurring.

Histology confirmed ligand capture and the specificity of viral expression: nearly all HTP-expressing cells (99.7%) were dopaminergic and most dopaminergic cells in the VTA (~64%) expressed HTP (**Extended Data Fig. 2f-h**). We did not opto-tag cells given concerns that overexpression of a second membrane protein could hinder surface trafficking of HTP. Instead, we identified putative dopamine neurons, as others have[41-43], by their unique electrophysiological features[44,45], criteria known to yield ~12% false-positives[45].

To further scrutinize the data, we used gabazine^{DART}'s impact on pauses as a proxy for HTP expression and ligand capture in individual cells. Reductions in the number of pauses corresponded with a decrease in pause length (Pearson's r^2=0.28, P=0.0006, **Extended Data Fig. 2i**), congruent with a pause-reduction effect. However, the median interspike interval showed no correlation to pause reduction (Pearson's r^2=0, P=0.95) while total spikes trended very weakly (Pearson's r^2=0.04, P=0.2, **Extended Data Fig. 2j**). Thus, the underlying tonic rhythm was unaffected, while subtle total-spike increments are an expected proxy of pause reduction itself. Finally, no correlations were found with respect to burst parameters (**Extended Data Fig. 2k**). Thus, gabazine^{DART} specifically reduces VTA_{DA} pauses, leaving tonic- and burst-firing characteristics intact.

Blocking $GABA_A$ receptors on VTA_{DA} cells accelerates Pavlovian extinction

Given that gabazine^{DART} prevents VTA_{DA} pauses, we expected it to slow extinction learning[14,22,23,29,30]. We tested this in water-deprived mice, trained for 10 days to associate cue A (2.5 kHz tone, 1.5 sec) with sucrose reward in a head-fixed configuration (**Fig. 2a-b**). Anticipatory licking during the cue (prior to reward delivery) served as the primary learning metric (**Fig. 2c-d**; **Extended Data Fig. 3a**). On day 11, mice received gabazine^{DART} and a 2 hr rest before resuming rewarded cue A trials for 15 min. Thereafter, Pavlovian extinction (unrewarded cue A trials) commenced, continuing into the final day (**Fig. 2e-f**, top). Contrary to expectations, we saw significantly accelerated extinction in $^{+}$HTP mice in comparison to ^{dd}HTP controls (P=0.0043, two-sided permutation test, **Fig. 2g**)—opposite the hypothesized direction of influence exerted by $GABA_A$ receptors on VTA_{DA} cells.

Mice were assayed during their dark (active) circadian phase, each being initially naïve to the task. To avoid motivational frustration from complete reward denial[46], cue A extinction trials were randomly interleaved with trials that paired a distinct cue B (11 kHz tone, 1.5 sec) with sucrose reward (**Fig. 2e-f**, bottom). This design maintained consistent overall reward availability, while affording a within-mouse measure of Pavlovian conditioning. This form of learning, which is believed to depend on VTA_{DA} bursts[12-21], was completely unaffected by gabazine^{DART} (P=0.53, $^{+}$HTP vs ^{dd}HTP, two-sided permutation test, **Fig. 2h**).

During training (days 1-10), we did not explicitly teach mice to discriminate cue B from cue A, as this can impede later learning via latent inhibition[47]. Instead, we trained mice to ignore environmental sounds other than cue A by imposing a timeout for licking during the random (3-13 sec) inter-trial interval (**Fig. 2b**). This approach allowed cue B to remain novel while achieving implicit cue discrimination in the vast majority of mice: 89% (24 of 27) were unresponsive to rare probes of cue B presented on day 10, despite robust anticipatory licking to cue A, thereby satisfying our behavioral inclusion criteria (**Extended Data Fig. 3b**).

Finally, after the session on day 12, every mouse underwent brain histology to quantify target engagement. Locomotor enhancements, known to occur with VTA_{DA} disinhibition[39,48-51], showed no correlation with gabazine^{DART} target engagement, nor with either form of Pavlovian learning (**Extended Data Fig. 3c-e**). By contrast, a significant correlation between Pavlovian extinction and gabazine^{DART} target engagement was seen (Pearson's r^2=0.36, P=0.04, **Extended Data Fig. 3f**), underscoring its dose-dependency.

VTA_{DA} dynamics during Pavlovian behavior

Given our surprising behavioral findings, we further scrutinized neural dynamics during the Pavlovian assay. Photometry recordings were obtained from medial VTA_{DA} neurons that co-expressed HTP and jGCaMP8f[52], a cytosolic protein optimized to detect rapid calcium decrements (**Fig. 3a**). Histology confirmed fiber placement, AAV co-expression, and ligand capture (**Fig. 3b, Extended Data Fig. 4a**). Of 18 mice that met behavioral criterion, 12 mice (6 experimental, 6 control) met a minimum signal-fidelity criterion (**Extended Data Fig. 4b**).

Control mice exhibited a canonical VTA_{DA} pause to reward omission (**Fig. 3c**, right, black). These pauses were prominent during early extinction trials and diminished quickly thereafter, aligning with observations of Kasai, Yagishita, and colleagues[30]. We thus focused on the first 4 extinction trials, and observed the elimination of pauses in $^{+}$HTP/gabazine^{DART} mice (**Fig. 3c**, pink data), with a pronounced statistical difference from controls (two-sided permutation test, P=0.001, **Fig. 3c**, center panel). In subsequent trials, VTA_{DA} pauses diminished in control mice, leaving no statistical difference to manipulated animals (P=0.658, **Fig. 3d**).

We saw no group differences before ligand infusion, nor post-gabazine^{DART} effects on baseline GCaMP signals (**Extended Data Fig. 4c-e**), consistent with the stable tonic firing seen in our electrical recordings (**Fig. 1f**). Likewise, bursts to cue A were not significantly altered (**Extended Data Fig. 4f-g**, left panels, **Fig. 1e**). Trends towards increased VTA_{DA} activity during cue B conditioning trials did not reach statistical significance (**Extended Data Fig. 4h**), consistent with unaltered behavioral conditioning (**Fig. 2h**). We also observed a biphasic burst-pause during early cue B and late cue A presentations (**Extended Data Fig. 4e-h**), as reported previously for cues that predict non-reward[25]. This burst-pause was insensitive to gabazine^{DART}, suggesting no $GABA_A$ receptor involvement. Finally, in agreement with Uchida and colleagues, we confirmed that GABA attenuates VTA_{DA} bursts to predictable rewards (P=0.034, **Extended Data Fig. 4f**, right inset).

These photometry results align with our earlier electrophysiology data, providing confidence in gabazine^{DART}'s specificity within the Pavlovian context. Beyond technical confirmation, our data support and enrich the GABA subtraction model put forth by Uchida and colleagues[15], wherein a GABA-encoded prediction either diminishes bursts if the reward is received (**Extended Data Fig. 4f**) or produces a pause if the reward fails to materialize (**Fig. 3c**). While these data confirm that $GABA_A$-mediated VTA_{DA} pauses encode worse-than-expected outcomes (**Fig. 3**), this correlative adherence to RPE belies a starkly different causal picture—one in which $GABA_A$-mediated VTA_{DA} pauses favor persistence over adaptation (**Fig. 2**).

Gabazine^{DART} impacts perseverative, but not flexible, mice

We observed a phenotypic spectrum across mice in which extinction was anti-correlated with conditioning in ^{dd}HTP controls (Pearson's r^2=0.73, P=0.0004, **Fig. 4a**, black). We used conditioning, given its insensitivity to gabazine^{DART}, to sort mice into upper and lower halves of the phenotypic spectrum. Slow-conditioning mice, sorted by their hesitance to learn the cue B association, exhibited rapid cue A extinction (**Fig. 4b**, black). Fast-conditioning mice, naturally quick to learn the cue B association, tended to perseverate, responding to cue A long after it ceased to predict reward (**Fig. 4c**, black).

Gabazine^{DART} eliminated perseveration in the fast-conditioning subset of mice, selectively accelerating extinction (P=0.001, two-sided permutation test, **Fig. 4e**) without altering their naturally rapid conditioning (P=0.8, **Fig. 4d**). Gabazine^{DART}, when administered to the other phenotypic category of mice, had little impact on either form of Pavlovian learning (**Fig. 4b**). Overall, gabazine^{DART} caused extinction to become uniformly rapid across the phenotypic spectrum, eliminating its anti-correlation with conditioning (Pearson's r^2=0.07, P=0.4, **Fig. 4a**, pink). Accordingly, a unique phenotype not seen in the control population emerged—mice adept at both rapid conditioning and rapid extinction (**Fig. 4c**, pink).

We did not see trending sex differences (**Fig. 4a**), nor any pattern in the randomly interleaved trials that could explain the behavioral differences across mice (**Extended Data Fig. 5a**), suggesting intrinsic trait variability as reported previously[53,54]. Although initial training rates did not predict an animal's later phenotype (**Extended Data Fig. 5b**), this could reflect variability in task familiarization rather than trait volatility. Finally, we consistently observed the same anti-correlation between conditioning and extinction across a larger set of 25 mice, pooled from the control arms of ongoing studies (**Extended Data Fig. 5c**). This underscores the unique rapid-conditioning / rapid-extinction phenotype produced by VTA_{DA}-specific $GABA_A$ antagonism (**Fig. 4c**, pink).

Discussion

Our work targeted VTA_{DA} neurons for their conceptually established dynamic components, which we sought to isolate via receptor-specific interventions. Prior manipulations of GABA release[34-36], $GABA_A$-specific pharmacology[33], and cell-specific optogenetic interventions[14,22-24,29,30] indicated that VTA_{DA} pauses serve to maintain or accelerate Pavlovian extinction, consistent with canonical models. With DART's dual cellular and pharmacological specificity, we corroborated a precise role for $GABA_A$ receptors in VTA_{DA} pause generation, with little impact on other aspects of neural firing. However, we observed behavioral effects diametrically opposite to canonical models—recasting $GABA_A$-mediated VTA_{DA} pauses from presumed catalysts of extinction to facilitators of behavioral persistence.

While seemingly contradictory, our findings offer complementary insights to previous studies. Widefield optical perturbations engage all VTA_{DA} cells synchronously, contrasting with gabazine^{DART}'s effects, which match the cellular and temporal pattern of GABA signaling events. Although both manipulations mitigate pauses on average, they exhibit distinct higher-order cellular and temporal dynamics. The sensitivity of extinction learning to these features suggests that the brain could strategically exploit these higher-order dynamics. For instance, VTA_{DA} pauses might manifest in various forms—allowing the $GABA_A$ pause to slow the rate of learning, while the canonical direction of learning is specified independently (**Supplementary Discussion**).

Regarding downstream implications, the strongest VTA_{DA} projection is to the striatum, where extinction learning has been attributed to indirect spiny projection neurons (iSPNs)[55,56]. At tonic dopamine levels, iSPNs exhibit two forms of spike-timing-dependent plasticity[57,58]—one of which is blocked by dopamine pauses[57,58]. This precedent, in which pauses can disable a form of learning, mirrors our behavioral findings, wherein natural $GABA_A$-mediated VTA_{DA} pauses slowed extinction learning in control ^{dd}HTP mice.

We and others have observed that VTA_{DA} pauses are uncommon events, limited to the first few failures of a previously dependable association[30,59] (**Fig. 3**); a context when persistence would be adaptive. However, the mechanism could become maladaptive if dysregulated. For instance, perseverative phenotypes are prevalent in schizophrenia[60], obsessive-compulsive disorder[61], post-traumatic stress disorder[62], addiction[63], Alzheimer's[64], and Parkinson's disease (PD)[65]. Because VTA_{DA} neurons are the last to degenerate in PD[66], they could contribute to the cognitive-rigidity symptoms of the disease, perhaps via $GABA_A$-mediated VTA_{DA} pauses. Further relevance to PD was seen in our prior study, which in light of our present work, implicates $GABA_A$-mediated VTA_{DA} pauses in slowing locomotion[39]. Notably, we saw no correlation between motor and non-motor changes in our present study, suggesting distinct underlying mechanisms (**Extended Data Fig. 3e-f**).

Beyond $GABA_A$, advances in targeted pharmacology will enable isolation of $GABA_B$ and other receptor-specific contributions to VTA_{DA} dynamics and animal behavior. Likewise, isolation of the presynaptic source of GABA is a future goal via subcellular[67] and synapse-specific[68] drug targeting. While much remains to be done, the precision of gabazine^{DART}, both in its specificity for extinction over conditioning behaviors and for perseverative over non-perseverative individuals (**Fig. 4**), underscores the potential of targeted circuit interventions for treating complex behaviors within a diverse population[69].

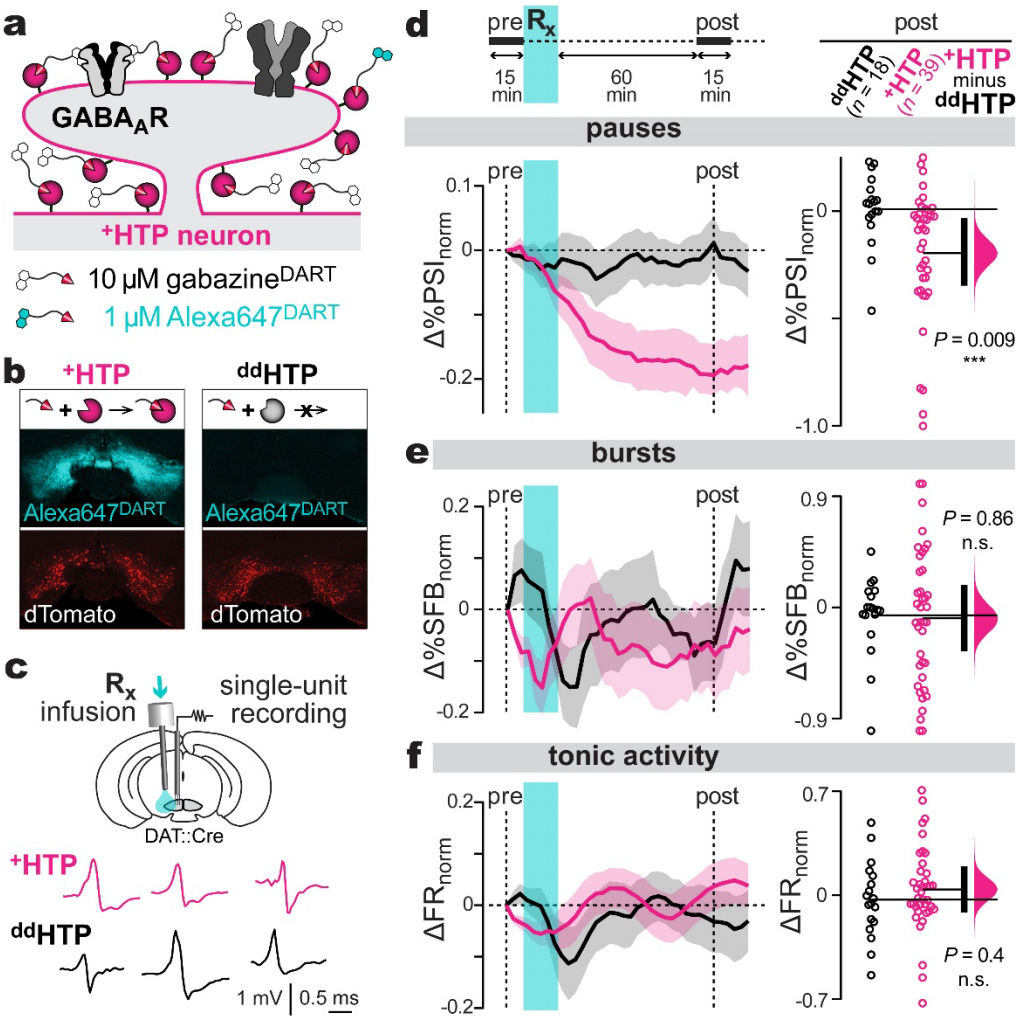

Fig. 1: GABA$_A$ receptors mediate VTA$_{DA}$ pauses *in vivo*

a: DART technology. AAV expression of the $^+$HTP protein (pink) enables cell-specific covalent capture of gabazine^{DART} (black) and Alexa647^{DART} (cyan) ligands. Once tethered, gabazine^{DART} blocks native GABA$_A$ receptors, while Alexa647^{DART} enables fluorescent visualization of target engagement.

b: Example histology. AAV expression of the active $^+$HTP or control ^{dd}HTP in VTA$_{DA}$ neurons is indicated by dTomato (red). All mice receive an intracranial ligand infusion of 10 μM gabazine^{DART} + 1 μM Alexa647^{DART}, and are perfused 36 hr later for histology. Alexa647^{DART} (cyan) quantifies ligand target engagement.

c: Electrophysiology. Top: an electrode bundle targeting the medial VTA enables *in vivo* extracellular recordings. A nearby cannula permits ligand infusion. **Bottom:** sample putative dopamine-neuron spikes, recorded in head-fixed animals, shown for $^+$HTP and ^{dd}HTP mice.

d: Pauses in firing: Top: time course of recording, spanning a baseline 15-min (pre-gabazine^{DART}) followed by infusion and post-gabazine^{DART} recording. **Bottom:** pause metric, $\%PSI$ (percent of interspike intervals longer than twice the median interspike interval). Changes in $\%PSI$ compare a 15-min baseline ($\%PSI_{pre}$) to a 15-min sliding window ($\%PSI_{post}$) according to $\Delta\%PSI_{norm} = (\%PSI_{post} - \%PSI_{pre}) / (\%PSI_{post} + \%PSI_{pre})$. **Left:** $\Delta\%PSI_{norm}$ time course, mean ± SEM over cells (n = 18 ^{dd}HTP cells, 3 mice; n = 39 $^+$HTP cells, 5 mice). **Right:** steady-state $\Delta\%PSI_{norm}$ (1-hr post-gabazine^{DART}) with individual cells (circles), group means (thin horizontal lines), mean-difference bootstrap (pink distribution), and 95% CI of the two-sided permutation test (vertical black bar); $^+$HTP and ^{dd}HTP cells differ significantly (P=0.009).

e-f: Burst/tonic firing: Analysis of $\%SFB$ (percent of spikes fired in bursts) and FR (firing rate) from the same cells; format as above.

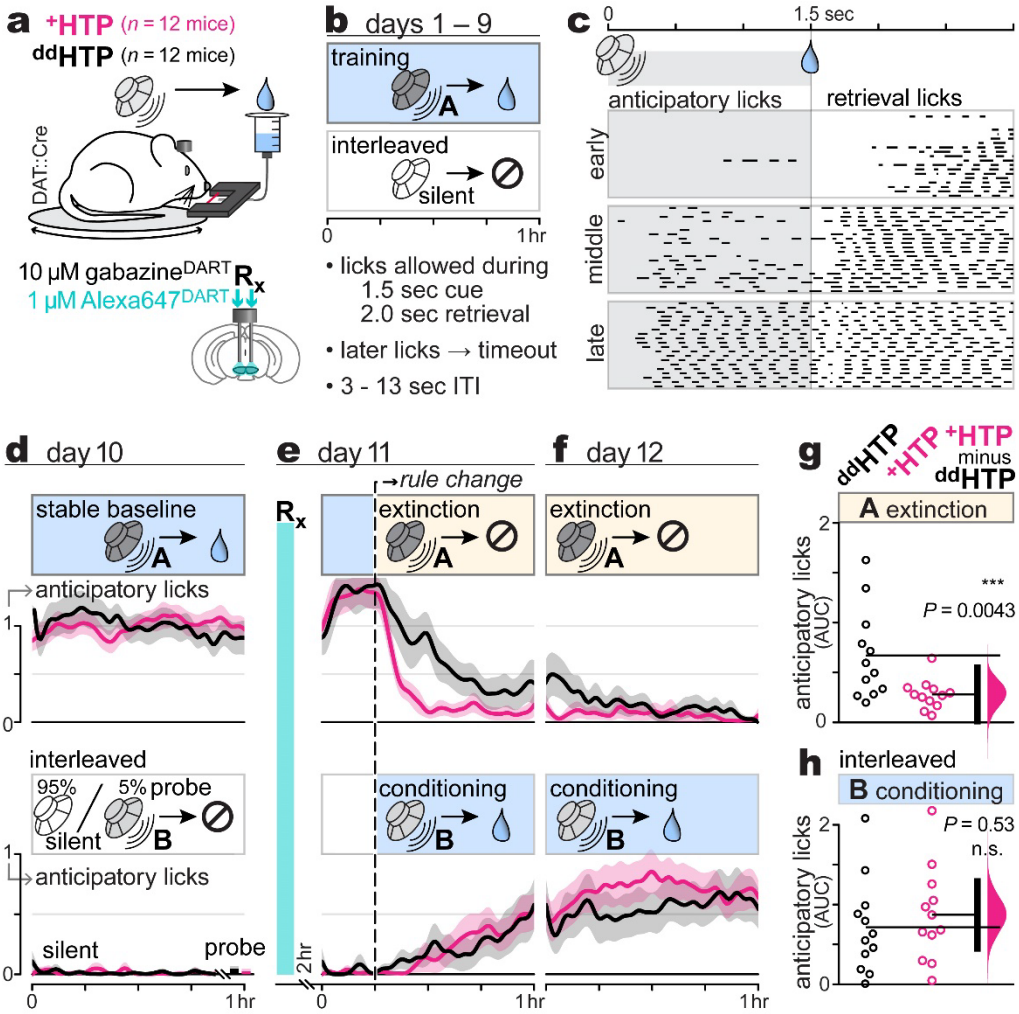

Fig. 2: Blocking $GABA_A$ receptors on VTA_{DA} cells accelerates Pavlovian extinction

a: Pavlovian behavior paradigm. DAT::Cre mice with a bilateral cannula in the VTA and $^{+}$HTP or ^{dd}HTP expression in VTA_{DA} cells. Mice are placed in a head-fixed configuration and presented with auditory cues and sucrose-water rewards. Licks are detected with an infrared beam, and locomotion is monitored via circular treadmill.

b: Training regimen. Over 9 days, mice undergo sessions where cue A (2.5 kHz tone, 1.5 sec) reliably signals reward, interspersed with silent trials (no cue, no reward) to monitor nonspecific licking. Licking during the random (3-13 sec) inter-trial interval is discouraged with a timeout, training mice to ignore environmental sounds other than cue A. Each session lasts 1 hour and comprises 100-150 cue A trials.

c: Anticipatory licking. Black line segments show beam breaks (licking) from a sample mouse on days 1 (early), 2 (middle), and 9 (late) of training.

d: Stable baseline. To account for individual-mouse differences, day 10 anticipatory licking to cue A is calculated for each mouse and used as a constant of normalization for that animal. The same normalization constant is applied to cue A trials (top) and silent / cue B trials (bottom). Lines and shading are the normalized anticipatory licking mean ± SEM over mice (n = 12 ^{dd}HTP mice; n = 12 $^{+}$HTP mice).

e-f: Pavlovian learning. On day 11, mice receive gabazine^{DART} and a 2 hr rest. The first ~15 min of the assay continue the prior day's rules. Following the rule change, unrewarded cue A trials (extinction) are randomly interleaved with rewarded cue B trials (conditioning), contingencies which continue into day 12. Lines and shading are $lick_{norm}$ mean ± SEM over mice (n = 12 ^{dd}HTP mice; n = 12 $^{+}$HTP mice).

g: Extinction *AUC* (area under the curve; $licks_{norm}$ × hr), integrating $lick_{norm}$ over 1.75 hr of Pavlovian learning (post rule-change). *AUC* = 1.75 indicates no extinction (cue A anticipatory licking equal to that on day 10), while smaller values indicate greater extinction. *AUC* of individual mice (circles), group means (thin horizontal lines), mean-difference bootstrap (pink distribution), and 95% CI of the two-sided permutation test (vertical black bar) indicate a significant difference between $^{+}$HTP and ^{dd}HTP mice (P=0.0043).

h: Conditioning *AUC*. Format as above, showing cue B conditioning trials from the same mice (P=0.53).

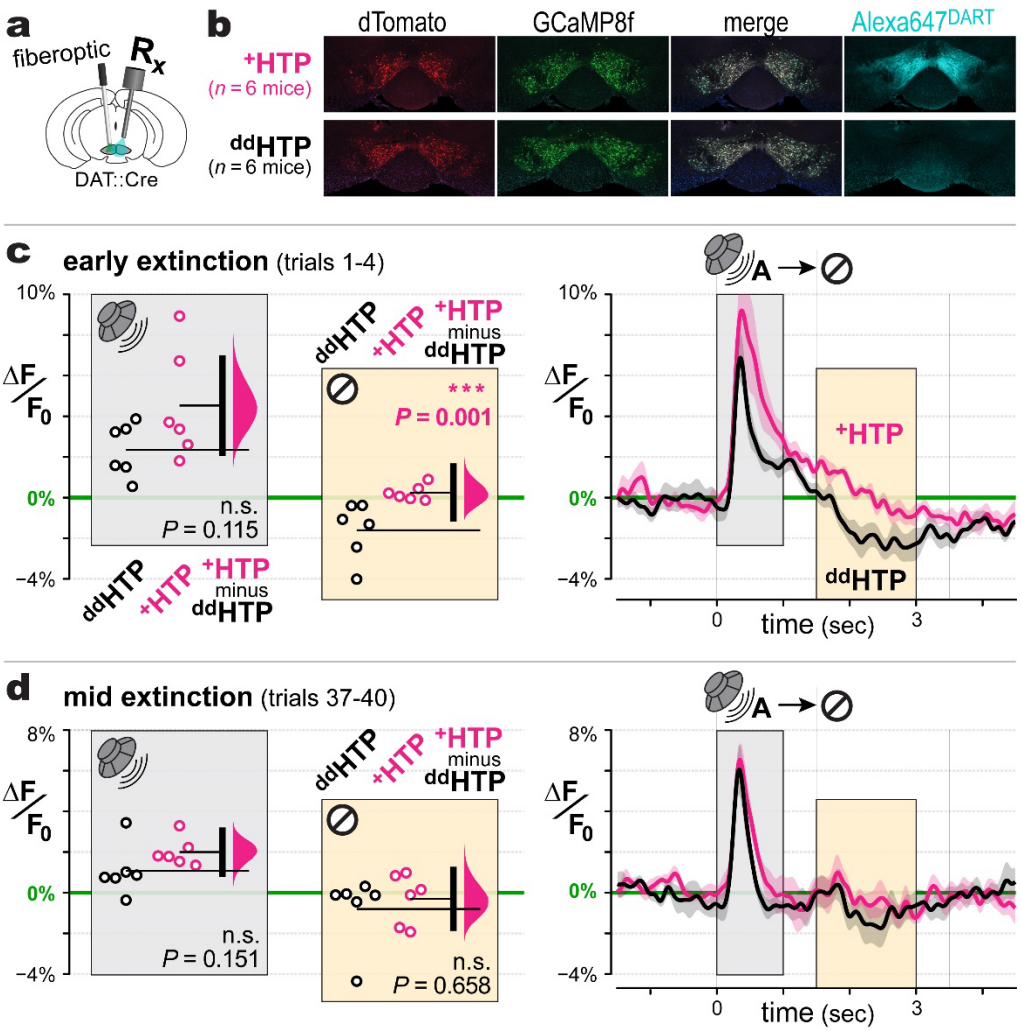

Fig. 3: VTA_{DA} dynamics during Pavlovian behavior

a: Experimental setup. DAT::cre mice injected with AAV-DIO-GCaMP8f and either AAV-DIO-$^{+}HTP_{GPI}$ or AAV-DIO-$^{dd}HTP_{GPI}$ in the VTA. Cannula and optical fiber implants permit intracranial DART infusions and calcium recording from VTA_{DA} neurons throughout the 12-day Pavlovian assay.

b: Example histology. AAV expression of GCaMP8f (green) and the active $^{+}$HTP or control ^{dd}HTP indicated by dTomato (red). All mice receive an intracranial ligand infusion of 10 μM gabazine^{DART} + 1 μM Alexa647^{DART}, and are perfused 36 hr later for histology. Alexa647^{DART} (cyan) quantifies ligand target engagement.

c: Early extinction. GCaMP8f responses in ^{dd}HTP (black) vs $^{+}$HTP (pink) mice during the first four extinction trials. **Right**: time course of $\Delta F/F_0$ mean ± SEM over mice (n = 6 ^{dd}HTP mice; n = 6 $^{+}$HTP mice). Analysis of $\Delta F/F_0$ during cue-burst (0 - 1 sec) and omission-pause (1.5 - 3 sec) is plotted in the left panel of corresponding color. **Left:** individual mice (circles), group means (thin horizontal lines), mean-difference bootstrap (pink distribution), and 95% CI of the two-sided permutation test (vertical black bar). $^{+}$HTP and ^{dd}HTP mice were not statistically different during cue Burst (P=0.115), yet differed significantly during omission-pause (P=0.001).

d: Middle extinction. Format as above, during extinction trials 37 – 40.

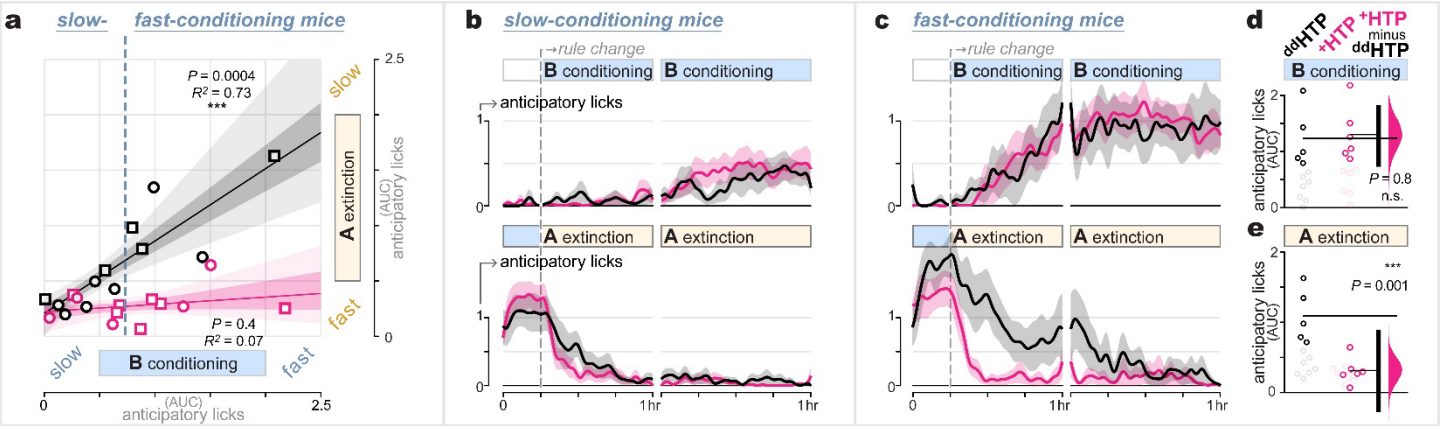

Fig. 4: Gabazine^{DART} impacts perseverative, but not flexible, mice

a: Phenotypic spectrum. Extinction-*AUC* vs conditioning-*AUC* measured within-mouse. Individual mice (squares = males, circles = females), regression fit (line), and regression 95% and 68% CI (light and dark shading) are shown for ^{dd}HTP (black, n = 12) and $^{+}$HTP (pink, n = 12) mice. In ^{dd}HTP mice, we observe an anti-correlation wherein fast-conditioning and slow-extinction (upper-right) tend to co-occur (Pearson's r^2 = 0.73, P = 0.0004). In $^{+}$HTP mice, the full spectrum of conditioning is seen, however extinction is uniformly rapid, independent of conditioning (Pearson's r^2 = 0.07, P = 0.4). Vertical dashed line illustrates the conditioning boundary (*AUC* = 0.75) chosen to divide mice into the approximate lower and upper halves of the phenotypic spectrum.

b: **Slow-conditioning mice**. Analysis of mice exhibiting slow conditioning (*AUC* < 0.75), with conditioning (top) and extinction (bottom). Lines and shading are normalized anticipatory licking, mean ± SEM over mice (n = 7 ^{dd}HTP mice; n = 6 $^{+}$HTP mice);

c: Fast-conditioning mice. Analysis of mice exhibiting fast conditioning (*AUC* > 0.75), with conditioning (top) and extinction (bottom). Lines and shading are normalized anticipatory licking and mean ± SEM over mice (n = 5 ^{dd}HTP mice; n = 6 $^{+}$HTP mice).

d-e: Fast-conditioning *AUC*. Summary data with the slow-conditioning subset of mice removed (faded circles), allowing a focused analysis of the fast-conditioning subset (*AUC* > 0.75). *AUC* of individual mice (circles), group means (thin horizontal lines), mean-difference bootstrap (pink distribution), and 95% CI of the two-sided permutation test (vertical black bar) indicate that $^{+}$HTP and ^{dd}HTP differ significantly with regard to extinction learning (P=0.001).

EXTENDED DATA FIGURES

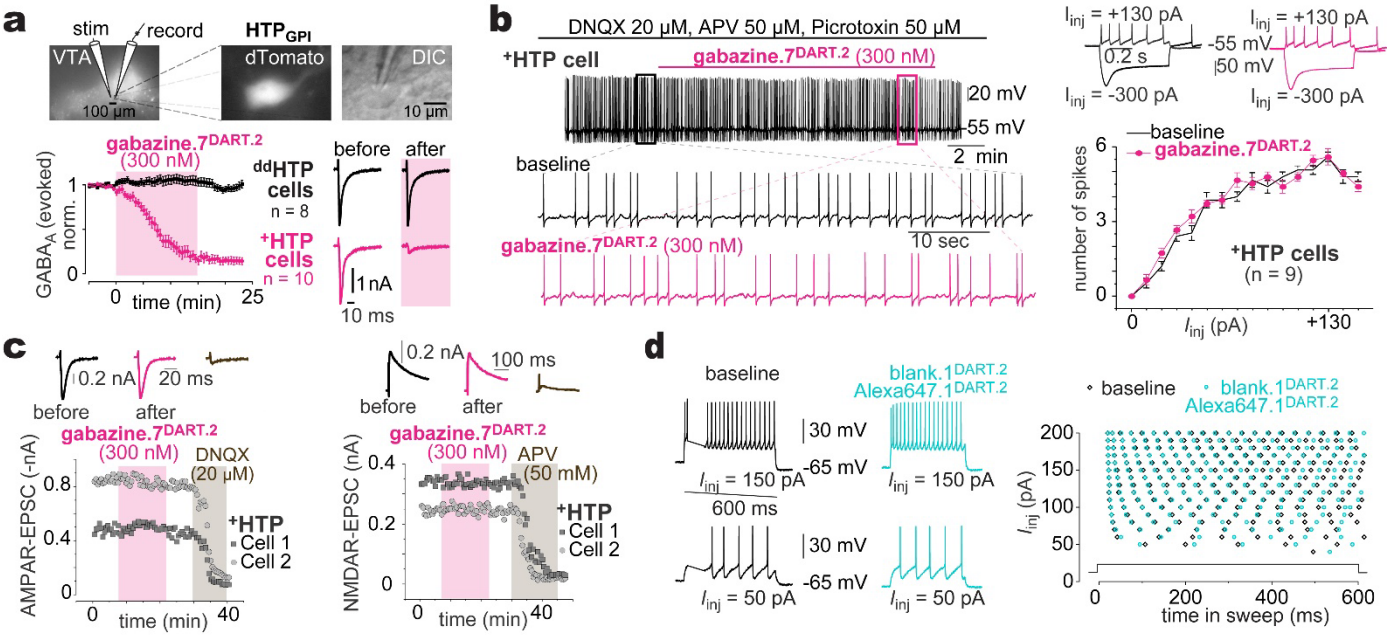

Extended Data Fig. 1: Specificity of gabazine^{DART} to the GABA$_A$R

a: Gabazine.7$^{DART.2}$ validation. Top: evoked-IPSC configuration in VTA slice. **Bottom:** 300 nM gabazine.7$^{DART.2}$ has no impact on ^{dd}HTP neurons, while blocking IPSCs on $^{+}$HTP cells in under 15 min (86 ± 4% block). Data are mean ±SEM, cells normalized to baseline ($^{+}$HTP: n=10 cells; ^{dd}HTP: n=8 cells). Example traces to right.

b: Gabazine.7$^{DART.2}$ and VTA$_{DA}$ action potentials. Left: current clamp of a VTA$_{DA}$ neuron in the presence of picrotoxin (GABA$_A$ receptor blocker), DNQX (AMPA receptor blocker), and APV (NMDA receptor blocker). **Right:** quantification of action potential firing as a function of injected current; performed before (black) vs after (cyan) gabazine.7$^{DART.2}$ was tethered in each cell. Representative traces shown above. Error bars are mean ±SEM over cells (*n* = 9).

c: Gabazine.7$^{DART.2}$ and AMPARs/NMDARs. Left: 300 nM gabazine.7$^{DART.2}$ has no effect on $^{+}$HTP neuron AMPAR-EPSCs, which are subsequently blocked by 20 µM DNQX. Example traces above. **Right:** 300 nm gabazine.7$^{DART.2}$ has no effect on $^{+}$HTP neuron NMDAR-EPSCs, which are subsequently blocked by 50 µM APV. Example traces above.

d: Alexa647.1$^{DART.2}$ validation. Current clamp studies in VTA$_{DA}$ $^{+}$HTP neurons with 10:1 blank.1$^{DART.2}$ + Alexa647.1$^{DART.2}$. No significant change was observed before vs after Alexa647.1$^{DART.2}$ was tethered. Representative traces shown left.

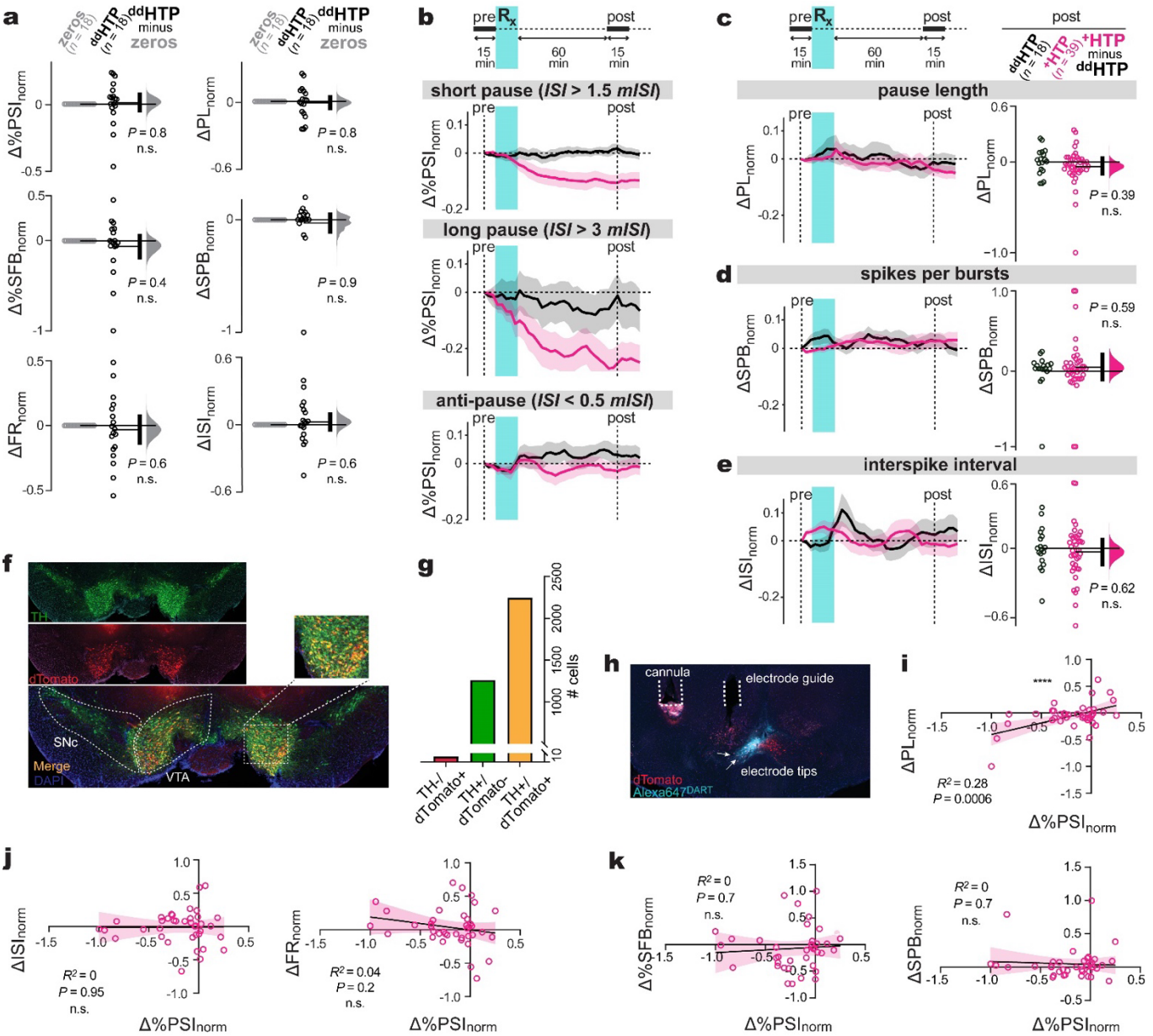

Extended Data Fig. 2: Supporting data for *in vivo* electrophysiology

a. Stability of control ddHTP metrics. Analysis of tonic, burst, and pause stability in ddHTP mice. Steady-state Δ_{norm} (1-hr post-gabazine^{DART}) with individual cells (circles), group means (thin horizontal lines), mean-difference bootstrap (grey distribution), and 95% CI of the two-sided permutation test (vertical black bar), comparing ddHTP cells to zero.

b. Pause result. Robustness analysis of our primary pause metric, ***%PSI***. The top two panels examine various "longer-than-average" metrics of pause occurrence (format as in **Fig. 1d**). The bottom panel examines a "shorter-than-average" metric to test for the asymmetry of effects.

c-e. Pause length, bursts, and ISI. Analysis of ***PL*** (pause length), ***SPB*** (spikes per burst), and ***mISI*** (median interspike interval); format as in **Fig. 1d-f**.

f-g. Cell counting. Representative histology and quantitative cell counting. Dopamine neurons (TH, tyrosine-hydroxylase, green). HTP expression (dTomato, red). Cell counting was performed from one representative brain. There were 2,244 double-labeled (dTomato$^+$/TH$^+$) cells. This represents 99.7% of all virus-positive cells (2,250 dTomato$^+$), and 64% of all dopaminergic cells (3,507 TH$^+$).

h. Electrode histology. Post-electrophysiology histology. HTP expression (dTomato, red); ligand capture (cyan); and electrode tips (arrows).

i. Pauses vs pause length. Correlation between ***PL*** (pause length) and ***%PSI*** from each $^+$HTP cell (circles, n=39), with regression ±95% CI (line and shading). Pearson's r^2 = 0.28, P = 0.0006.

j-k. Pauses vs other features. Correlation between all other metrics and ***%PSI***; format as above.

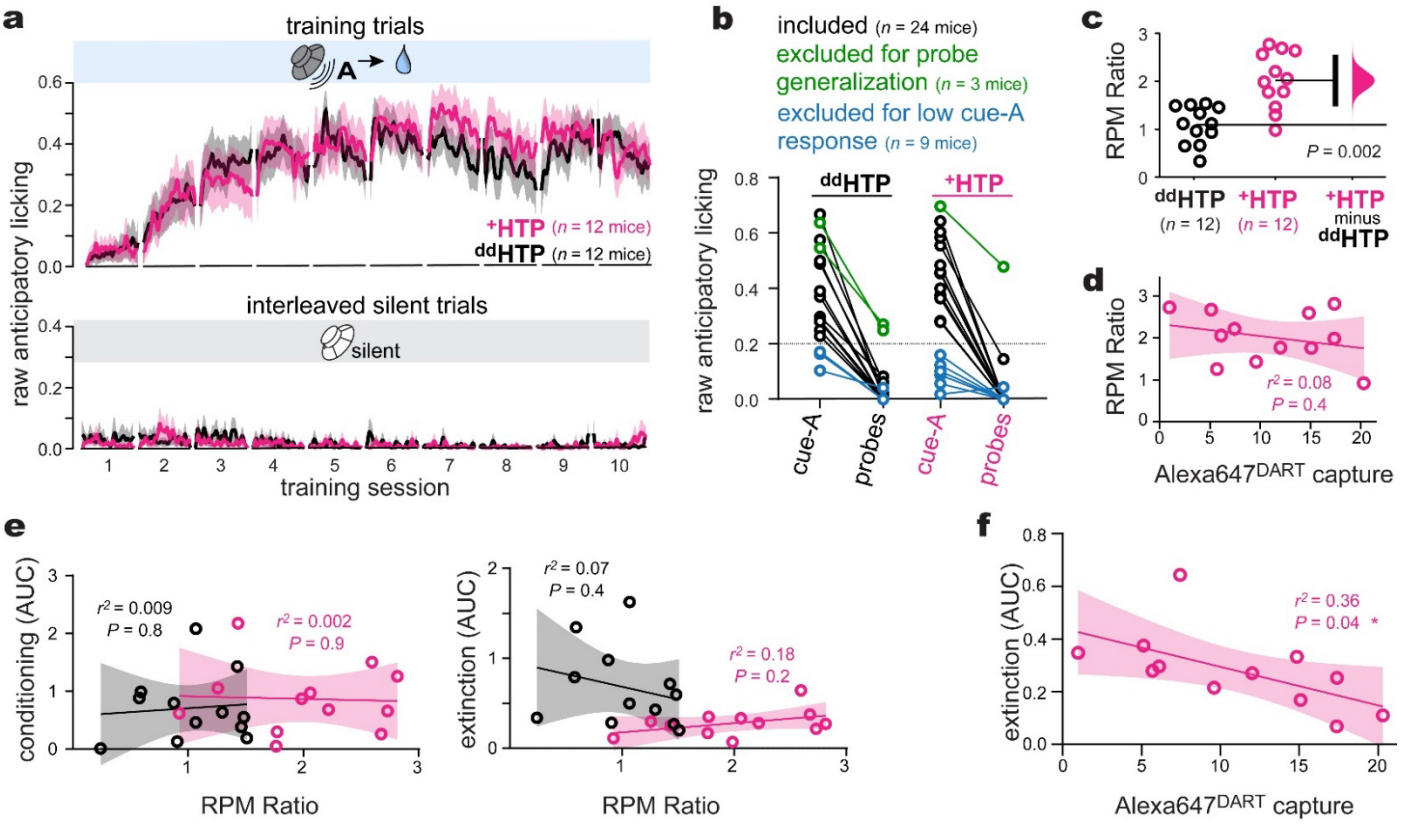

Extended Data Fig. 3: Supporting data for Pavlovian extinction and conditioning assay

a. Training sessions. Lines and shading show the raw (non-normalized) anticipatory licking (fraction of time that beam is broken during the cue), mean ± SEM over mice (n = 12 ^{dd}HTP; n = 12 $^{+}$HTP). Both $^{+}$HTP and ^{dd}HTP mice develop robust anticipatory licking to cue A across training, while exhibiting little to no background licking during silent trials.

b. Behavioral inclusion criteria. We required robust anticipatory licking to cue A (raw anticipatory licking greater than 0.2) and low responsiveness to cue B probes (less than 30% of cue A anticipatory licking). A total of 9 mice (3 ^{dd}HTP and 6 $^{+}$HTP) were excluded for lack of cue A responsiveness (blue). Of the remaining 27 mice, only 3 mice (2 ^{dd}HTP and 1 $^{+}$HTP) were excluded for probe generalization (green). Thus 89% (24 of 27) successfully discriminated cue B.

c. Locomotion. Ratio of the average treadmill RPM post-gabazine^{DART} (day 11-12) divided by pre-gabazineDART (day 8-10). Individual mice (circles), group means (thin horizontal lines), mean-difference bootstrap (pink distribution), and 95% CI of the two-sided permutation test (vertical black bar). As previously reported[39], disinhibition of VTA_{DA} neurons enhances locomotion.

d. Locomotion vs histology. Correlation between RPM ratio and Alexa647^{DART} capture in the dorsal VTA of $^{+}$HTP mice (n=12). Mice (circles), regression ±95% CI (line and shading). Pearson's r^2 = 0.08, P = 0.4 indicates no significant correlation.

e. Locomotion vs reward learning. Correlation between RPM ratio and our two measures of reward learning: conditioning AUC (left) and extinction AUC (right). Mice (circles; n=12 ^{dd}HTP; n=12 $^{+}$HTP) and regression ±95% CI (line and shading). Pearson's tests show no significant correlation (r^2 and P values as indicated).

f. Extinction learning vs histology. Correlation between extinction (AUC) and Alexa647^{DART} capture in the dorsal VTA of $^{+}$HTP mice (n=12). Mice (circles), regression ±95% CI (line and shading). Pearson's r^2 = 0.36, P = 0.04 indicates a significant correlation, with higher levels of target engagement corresponding to faster rates of extinction.

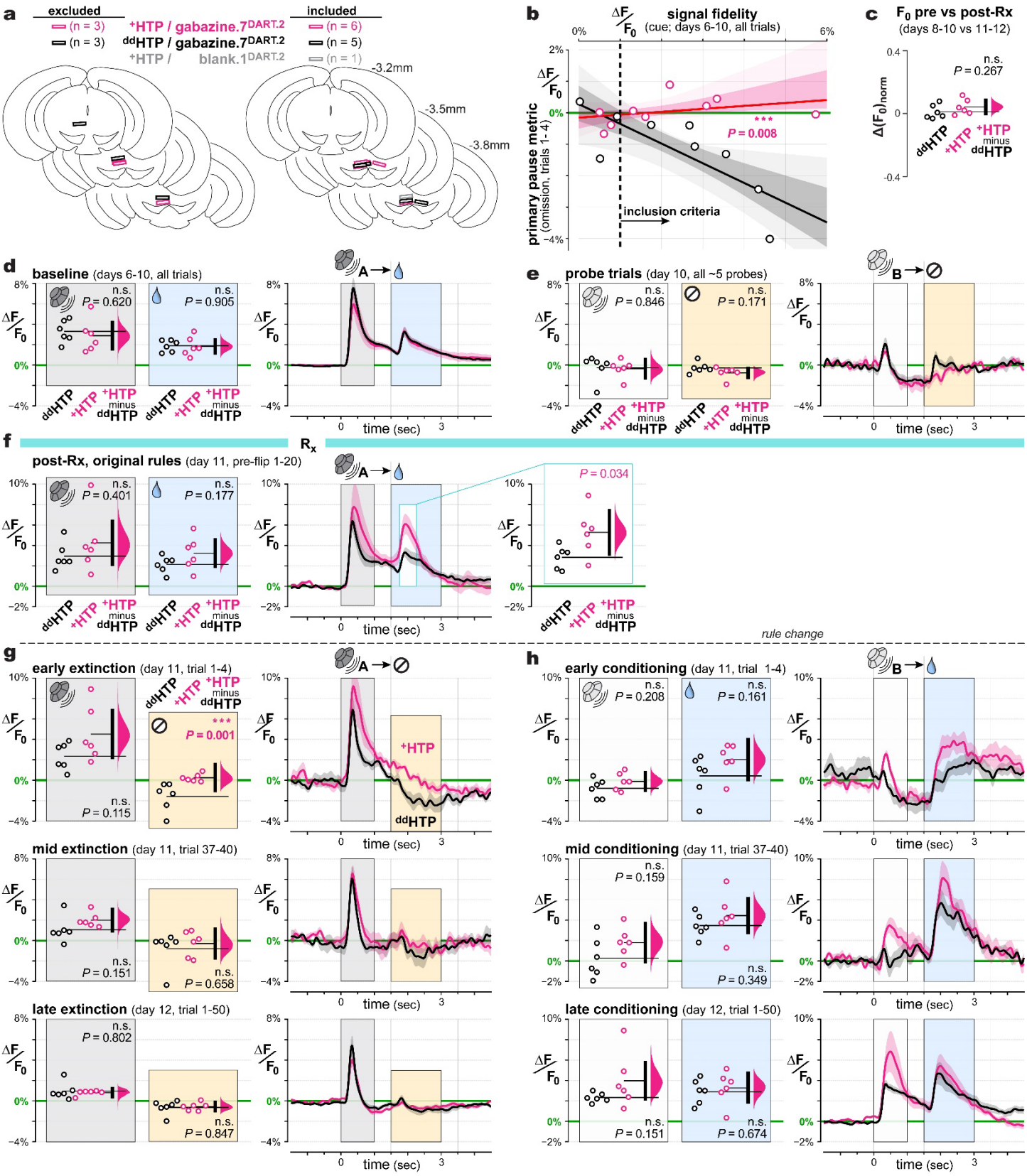

(legend on next page)

Extended Data Fig. 4: Supporting data for fiber photometry studies

a: Fiber placement. Optic fibers were placed dorsal to the VTA and equivalently spread between control and experimental conditions. 6 mice (3 $^{+}$HTP/gabazine^{DART} and 3 ^{dd}HTP/gabazine^{DART}) were excluded based on GCaMP8f signal levels (left). 12 mice (6 $^{+}$HTP/gabazine^{DART}, 5 ^{dd}HTP/gabazine^{DART}, and 1 $^{+}$HTP/blank^{DART}) were included in further analysis (right).

b: Photometry inclusion criteria. Signal-fidelity metric (cue-evoked burst, days 6-10) reflects GCaMP8f expression and its coupling efficiency to the fiber-optic. This pre-gabazine^{DART} signal-fidelity metric is plotted against our main post-gabazine^{DART} pause metric (omission pause, day 11 extinction trials 1-4). Data from individual mice (circles), regression fits (lines), and regression 95% and 68% CI (light and dark shading) are shown for ^{dd}HTP (black, n = 9) and $^{+}$HTP (pink, n = 9) mice. With all data included, there is a clear statistical difference between ^{dd}HTP and $^{+}$HTP mice (two-sided permutation slope test, P = 0.008). Mice above a signal-fidelity threshold (to the right of the dashed line at 1% $\Delta F/F_0$) are included in the subsequent analyses.

c. Tonic activity. Changes in baseline GCaMP8f intensity on days 8-10 ($F_{0,pre}$) vs days 11-12 ($F_{0,post}$) are analyzed according to $\Delta(F_0)_{norm} = (F_{0,post} - F_{0,pre}) / (F_{0,post} + F_{0,pre})$. Individual mice (circles), group means (thin horizontal lines), mean-difference bootstrap (pink distribution), and 95% CI of the two-sided permutation test (vertical black bar); $^{+}$HTP and ^{dd}HTP cells do not differ significantly (P=0.267).

d: Days 6-10 rewarded cue A trials. Right: GCaMP8f responses in ^{dd}HTP (black) vs $^{+}$HTP (pink) mice during days 6-10 (average over all cue A trials). Right panel shows the time course of $\Delta F/F_0$ mean ± SEM over mice (n = 6 ^{dd}HTP mice; n = 6 $^{+}$HTP mice). Analysis of $\Delta F/F_0$ during cue (gray) and reward (yellow) is plotted in the left panel of corresponding color. **Left:** individual mice (circles), group means (thin horizontal lines), mean-difference bootstrap (pink distribution), and 95% CI of the two-sided permutation test (vertical black bar). $^{+}$HTP and ^{dd}HTP mice were not statistically different during cue (0 – 1 sec interval; P=0.620) or reward (1.5 – 3 sec interval, P=0.905). Examination of an additional, narrow-time reward interval (1.75 – 2.25 sec) was also not significant (P=0.968; not shown).

e: Day 10 unrewarded cue B probes. Format as in panel **d**; for pre-gabazine^{DART} unrewarded cue B probes. Cue-evoked signals (0 - 1 sec) were not statistically different in $^{+}$HTP vs ^{dd}HTP mice (P=0.846). Signals in the unrewarded interval displayed a non-significant trend (1.5 - 3 sec; P=0.171), which remained non-significant over a narrow interval (1.75 – 2.25 sec; P=0.054; not shown).

f: Day 11 rewarded cue A trials. Format as in panel **d**; post-gabazine^{DART} rewarded cue A trials (prior to rule change). Cue-evoked signals (0 - 1 sec) were not statistically different in $^{+}$HTP vs ^{dd}HTP mice (P=0.401). For reward-evoked signals, $^{+}$HTP mice exhibited a trending increase (1.5 - 3 sec; P=0.117) which was weakly significant within a narrow interval (1.75 – 2.25 sec; P=0.034, right inset).

g: Days 11-12 cue A extinction. Format as in panel **d**; post-gabazine^{DART} cue A extinction (early, middle, and late trials from top to bottom). Cue-evoked signals (0 - 1 sec) showed a non-significant trend during early (P=0.115) and middle (P=0.151) but not late (P=0.802) trials. Omission-pause signals (1.5 - 3 sec) were evident in ^{dd}HTP mice yet absent in $^{+}$HTP mice during early trials (P=0.001). This difference was not apparent during middle (P=0.658) and late (P=0.847) trials owing to the lack of pauses in control mice. Examination of a narrow interval (1.75 – 2.25 sec) upheld these results (early P=0.00045; middle P=0.448; late P=0.945).

h: Days 11-12 cue B conditioning. Format as in panel **d**; post-gabazine^{DART} cue B conditioning (early, middle, and late trials from top to bottom). Cue-evoked signals (0 - 1 sec) showed a non-significant trend (early P=0.208; middle P=0.159; late P=0.151). Reward-evoked signals displayed a similar trend for both the full (1.5 - 3 sec) interval (early P=0.161; middle P=0.349; late P=0.674) and narrow (1.75 – 2.25 sec) interval (early P=0.123; middle P=0.306; late P=0.640).

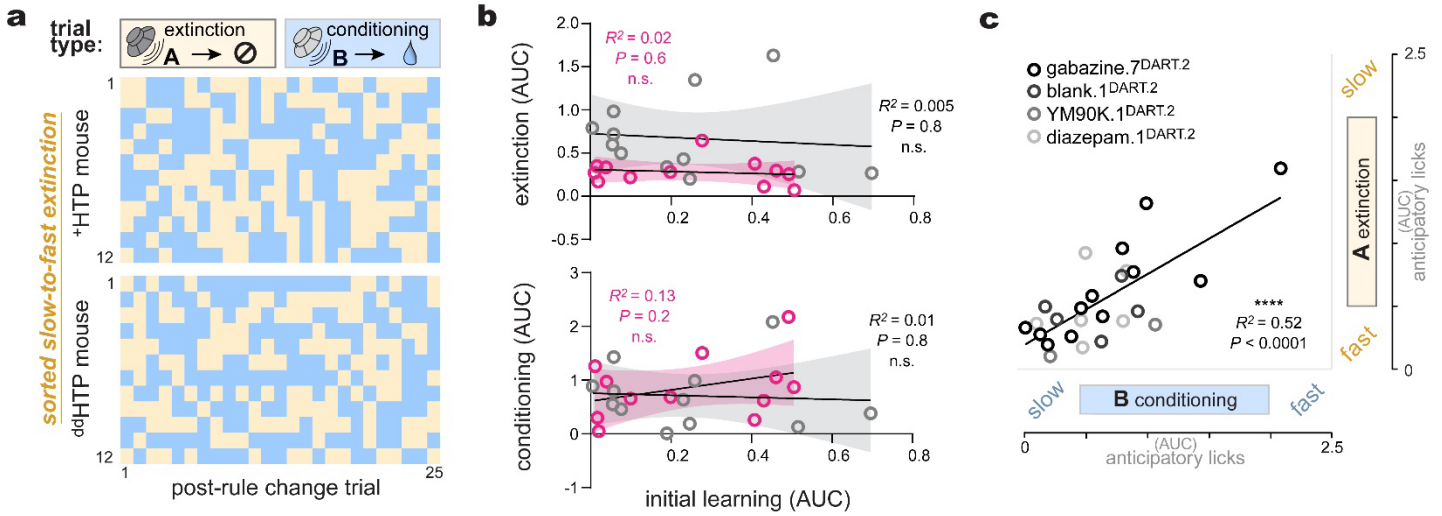

Extended Data Fig. 5: Supporting data for within-mouse behavioral correlations

a: Visual inspection of random order of interleaved trials. Each row is one mouse, sorted by extinction from the slowest to fastest (top to bottom). Columns indicate the first 25 trials after the rule-change, with trial type indicated by color (yellow = cue A extinction, blue = cue B conditioning). No visually discernable pattern is apparent in either $^{+}$HTP mice (n=12) or ^{dd}HTP mice (n=12).

b. Initial training vs later reward learning. Correlation between initial learning rates (AUC over training days 1-2) and our two measures of reward learning: extinction AUC (top) and conditioning AUC (bottom). Mice (circles; *n*=12 ^{dd}HTP; *n*=12 $^{+}$HTP) and regression ±95% CI (line and shading). Pearson's tests show no significant correlation (r^2 and *P* values as indicated).

c: Phenotypic spectrum across pooled controls. Conditioning-*AUC* vs extinction-*AUC* measured within-mouse. Individual mice (circles), regression fit (line), are shown for mice pooled from ongoing control experiments. All data are from ^{dd}HTP mice infused with various ligands, including gabazine.7$^{DART.2}$, blank.1$^{DART.2}$, YM90K.1$^{DART.2}$, or diazepam.1$^{DART.2}$. Pearson's r^2=0.52, *P*<0.0001.

Supplementary Discussion

In reinforcement models, the direction of learning is governed by δ, the reward prediction error (RPE), while the rate of learning is controlled by α. The product of these variables determines the overall learning per trial, as depicted in **Fig. S1**. It is important to note that this figure is not a representation of a specific reinforcement learning model, but rather serves to illustrate the multiplication of δ and α. Thus, the discussion below can be applied to any reinforcement model that incorporates these basic variables.

Traditionally, dopamine encodes δ exclusively, while the learning rate is held fixed. Thus, if a worse-than-expected RPE occurs (e.g., δ = -2) it is multiplied by the fixed learning rate (e.g., α = 1%) to determine the extent of extinction learning ($\delta \cdot \alpha$ = -2%).

We initially hypothesized that gabazine^{DART} would counteract worse-than-expected RPE signals (e.g., alter δ from -2 to -1) and thereby slow extinction learning. Surprisingly, our behavioral data revealed the opposite—a nearly threefold acceleration (requiring $\delta \cdot \alpha$ = -6%).

One plausible explanation for such acceleration by gabazine^{DART} could involve an increase in the rate parameter, α (an intervention indicated by the dashed pink arrow). This has two conceptual implications. Firstly, $GABA_A$-mediated VTA_{DA} pauses would primarily reduce α (illustrated by the dashed green arrow, which is equal and opposite to the pink arrow). Secondly, it suggests the existence of a distinct signal encoding the negative δ (depicted by the brown "non-$GABA_A$" arrow; orthogonal to the "$GABA_A$" arrow by definition).

This framework also coheres with optogenetic studies. In particular, 5-Hz excitatory stimulation had no impact on extinction learning[30], consistent with a modest increase in both parameters, which allows their product to remain unchanged (e.g., from the circle at δ = -2, α = 1% to the smaller white circle at δ = -1, α = 2%). However, a stronger perturbation in the same direction would eliminate extinction learning (gray circle at δ = 0, α = 3%), consistent with the 20-Hz perturbation studies[14,29,30].

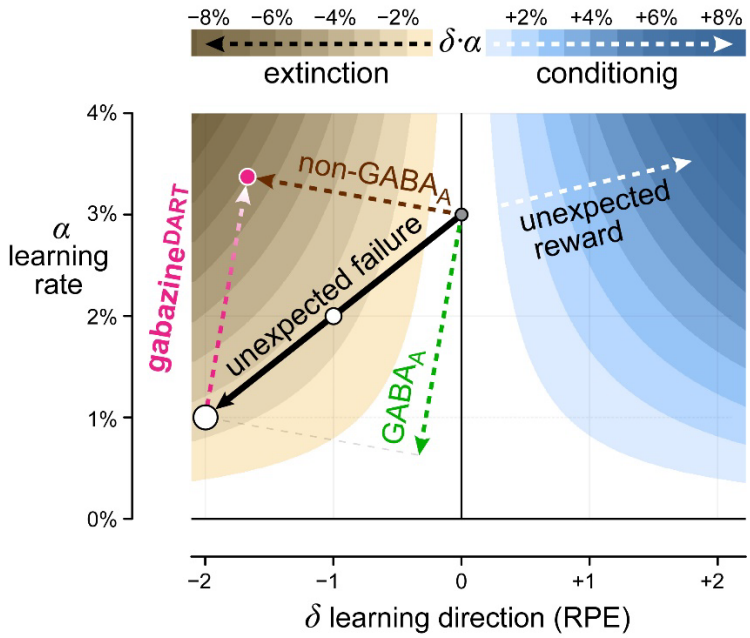

Fig. S1: Exploring learning direction vs rate. This figure illustrates the multiplication of two variables. We allow δ to vary from -2 to +2 (negative to positive RPE), while α varies from 0% to 4% (slow to fast). The value of their product is indicated by the color map. The chosen range of values is arbitrary and does not imply a specific model.

We can only speculate on the perturbation of VTA_{DA} action potentials needed to mimic gabazine^{DART}'s effects. Perhaps one would need to target a specific subset of VTA_{DA} cells whose outputs are specialized to influence α—a scenario implying an unusually specific role for $GABA_A$ receptors in only these cells. A more plausible scenario could involve higher-order temporal correlations. For instance, it may be necessary to match the precise timing of a given VTA_{DA} cell's pause, relative to activity in cells elsewhere in the brain. Synaptic plasticity is known to be gated by fine-scale temporal relationships, and $GABA_A$ can convey information on the millisecond timescale[9,70,71]. Nevertheless, these scenarios would pose challenges for direct testing. In the former scenario, identifying the correct cells, particularly given the unreliable occurrence of VTA_{DA} pauses on any given trial[28], would be unclear. The latter scenario would be even more challenging, considering the difficulty in predicting precisely when a $GABA_A$ pause will occur with millisecond precision.

Placing our findings in a broader context, α has been shown to vary based on attention, uncertainty, or surprise[72]. Mechanistically, these functions have been predominantly attributed to other neuromodulator systems, including acetylcholine, norepinephrine and serotonin[73]. A recent study found that dopamine may encode the learning rate during positive RPE policy learning; a form of motor learning in which mice fine-tune their kinematic strategy[21]. However, the study did not extend to negative RPE signals, nor to value learning, which were the focus of our study. Moreover, while surprising events typically cause α to increase[74], our findings present a paradoxical observation in which surprising failures caused α to decrease. This suggests a process akin to disbelief or stubbornness rather than the accelerated learning typically associated with surprise[75].

Acknowledgements

We would like to thank Isaac Weaver and Janani Sundararajan for help designing and building the behavioral assay; Ankit Choudhury for performing tyrosine hydroxylase immunostaining; Konstantin Bakhurin for providing training on implanting electrodes into the VTA; and Robin Blazing for providing training on spike sorting. We also thank Rich Mooney, Nicole Calakos, Mark Harnett, Elias Issa, Steve Lisberger, Erin Calipari, and Josh Dudman for insightful feedback on the manuscript. This work was supported by Duke University Startup Funds (MRT), NIH grants RF1-MH117055 and DP2-MH1194025 (MRT), and by the joint efforts of The Michael J. Fox Foundation for Parkinson's Research (MJFF) and the Aligning Science Across Parkinson's (ASAP) initiative. MJFF administers grant ASAP-020607 on behalf of ASAP and itself.

Author Contributions

See **Table S2** for detailed author contributions. **Conceptualization:** SCVB, MRT. **Methodology:** SCVB, HY, SSXL, BCS, MRT. **Software:** SCVB, MRT. **Validation:** SCVB, HY, SSXL, BCS, MRT. **Formal Analysis:** SCVB, HY, MRT. **Investigation:** SCVB, HY. **Resources:** HY, SSXL, BCS, MRT. **Data Curation:** SCVB. **Writing, Original Draft:** SCVB. **Writing, Review and Editing:** SCVB, HY, SSXL, BCS, MRT. **Visualization:** SCVB, HY, MRT. **Supervision:** MRT. **Project Administration:** SCVB, BCS, MRT. **Funding Acquisition:** MRT.

Competing Interests

MRT and BCS are on patent applications describing DART. Other authors declare no competing interests.

IP Rights Notice

For the purpose of open access, the author has applied a CC-BY public copyright license to the Author Accepted Manuscript (AAM) version arising from this submission.

References

1 Sandson, J. & Albert, M. L. Varieties of perseveration. *Neuropsychologia* **22**, 715-732 (1984).

2 Goodman, J. & Packard, M. G. There is more than one kind of extinction learning. *Frontiers in Systems Neuroscience* **13**, 16 (2019).

3 Bouton, M. E., Maren, S. & McNally, G. P. Behavioral and neurobiological mechanisms of pavlovian and instrumental extinction learning. *Physiological reviews* **101**, 611-681 (2021).

4 Schultz, W., Dayan, P. & Montague, P. R. A neural substrate of prediction and reward. *Science* **275**, 1593-1599 (1997).

5 Watabe-Uchida, M., Eshel, N. & Uchida, N. Neural circuitry of reward prediction error. *Annual review of neuroscience* **40**, 373-394 (2017).

6 Berke, J. D. What does dopamine mean? *Nature neuroscience* **21**, 787-793 (2018).

7 Cox, J. & Witten, I. B. Striatal circuits for reward learning and decision-making. *Nature Reviews Neuroscience* **20**, 482-494 (2019).

8 Tian, J. & Uchida, N. Habenula lesions reveal that multiple mechanisms underlie dopamine prediction errors. *Neuron* **87**, 1304-1316 (2015).

9 Shikano, Y., Yagishita, S., Tanaka, K. F. & Takata, N. Slow-rising and fast-falling dopaminergic dynamics jointly adjust negative prediction error in the ventral striatum. *European Journal of Neuroscience* **58**, 4502-4522 (2023).

10 Dabney, W. *et al.* A distributional code for value in dopamine-based reinforcement learning. *Nature* **577**, 671-675 (2020).

11 Hamid, A. A. *et al.* Mesolimbic dopamine signals the value of work. *Nature neuroscience* **19**, 117-126 (2016).

12 Tsai, H. C. *et al.* Phasic firing in dopaminergic neurons is sufficient for behavioral conditioning. *Science* **324**, 1080-1084 (2009). https://doi.org/10.1126/science.1168878

13 Witten, I. B. *et al.* Recombinase-driver rat lines: tools, techniques, and optogenetic application to dopamine-mediated reinforcement. *Neuron* **72**, 721-733 (2011).

14 Steinberg, E. E. *et al.* A causal link between prediction errors, dopamine neurons and learning. *Nature neuroscience* **16**, 966-973 (2013).

15 Eshel, N. *et al.* Arithmetic and local circuitry underlying dopamine prediction errors. *Nature* **525**, 243-246 (2015).

16 Chang, C. Y., Gardner, M., Di Tillio, M. G. & Schoenbaum, G. Optogenetic blockade of dopamine transients prevents learning induced by changes in reward features. *Current Biology* **27**, 3480-3486. e3483 (2017).

17 Sharpe, M. J. *et al.* Dopamine transients are sufficient and necessary for acquisition of model-based associations. *Nature Neuroscience* **20**, 735-742 (2017).

18 Saunders, B. T., Richard, J. M., Margolis, E. B. & Janak, P. H. Dopamine neurons create Pavlovian conditioned stimuli with circuit-defined motivational properties. *Nature neuroscience* **21**, 1072-1083 (2018).

19 Kutlu, M. G. *et al.* Dopamine release in the nucleus accumbens core signals perceived saliency. *Current Biology* **31**, 4748-4761. e4748 (2021).

20 Jeong, H. *et al.* Mesolimbic dopamine release conveys causal associations. *Science* **378**, eabq6740 (2022).

21 Coddington, L. T., Lindo, S. E. & Dudman, J. T. Mesolimbic dopamine adapts the rate of learning from action. *Nature* **614**, 294-302 (2023).

22 Danjo, T., Yoshimi, K., Funabiki, K., Yawata, S. & Nakanishi, S. Aversive behavior induced by optogenetic inactivation of ventral tegmental area dopamine neurons is mediated by dopamine D2 receptors in the nucleus accumbens. *Proceedings of the National Academy of Sciences* **111**, 6455-6460 (2014).

23 Chang, C. Y. *et al.* Brief optogenetic inhibition of dopamine neurons mimics endogenous negative reward prediction errors. *Nature neuroscience* **19**, 111-116 (2016).

24 van Zessen, R. *et al.* Cue and reward evoked dopamine activity is necessary for maintaining learned Pavlovian associations. *Journal of Neuroscience* **41**, 5004-5014 (2021).

25 Schultz, W. Predictive reward signal of dopamine neurons. *Journal of neurophysiology* (1998).

26 Cohen, J. Y., Haesler, S., Vong, L., Lowell, B. B. & Uchida, N. Neuron-type specific signals for reward and punishment in the ventral tegmental area. *nature* **482**, 85 (2012).

27 Engelhard, B. *et al.* Specialized coding of sensory, motor and cognitive variables in VTA dopamine neurons. *Nature* **570**, 509-513 (2019).

28 Fleming, W., Jewell, S., Engelhard, B., Witten, D. M. & Witten, I. B. Inferring spikes from calcium imaging in dopamine neurons. *PloS one* **16**, e0252345 (2021).

29 Lee, K. *et al.* Temporally restricted dopaminergic control of reward-conditioned movements. *Nature neuroscience* **23**, 209-216 (2020).

30 Iino, Y. *et al.* Dopamine D2 receptors in discrimination learning and spine enlargement. *Nature* **579**, 555-560 (2020).

31 Marshel, J. H. *et al.* Cortical layer–specific critical dynamics triggering perception. *Science* **365**, eaaw5202 (2019).

32 Fan, L. Z. *et al.* All-optical physiology resolves a synaptic basis for behavioral timescale plasticity. *Cell* **186**, 543-559. e519 (2023).

33 Pan, W.-X., Schmidt, R., Wickens, J. R. & Hyland, B. I. Tripartite mechanism of extinction suggested by dopamine neuron activity and temporal difference model. *Journal of Neuroscience* **28**, 9619-9631 (2008).

34 Tan, K. R. *et al.* GABA neurons of the VTA drive conditioned place aversion. *Neuron* **73**, 1173-1183 (2012). https://doi.org/10.1016/j.neuron.2012.02.015

35 Van Zessen, R., Phillips, J. L., Budygin, E. A. & Stuber, G. D. Activation of VTA GABA neurons disrupts reward consumption. *Neuron* **73**, 1184-1194 (2012).

36 Rost, B. R., Wietek, J., Yizhar, O. & Schmitz, D. Optogenetics at the presynapse. *Nat Neurosci* **25**, 984-998 (2022). https://doi.org/10.1038/s41593-022-01113-6

37 Parker, J. G. *et al.* Attenuating GABAA receptor signaling in dopamine neurons selectively enhances reward learning and alters risk preference in mice. *Journal of Neuroscience* **31**, 17103-17112 (2011).

38 Shields, B. C. *et al.* Deconstructing behavioral neuropharmacology with cellular specificity. *Science* **356**, eaaj2161 (2017).

39 Shields, B. C. *et al.* Thousandfold Cell-Specific Pharmacology of Neurotransmission. *BioRxiv*, 2022.2010.2018.512779 (2022).

40 Lobb, C. J., Wilson, C. J. & Paladini, C. A. A dynamic role for GABA receptors on the firing pattern of midbrain dopaminergic neurons. *Journal of neurophysiology* **104**, 403-413 (2010).

41 Salinas-Hernández, X. I. *et al.* Dopamine neurons drive fear extinction learning by signaling the omission of expected aversive outcomes. *Elife* **7**, e38818 (2018).

42 Pan, W.-X., Coddington, L. T. & Dudman, J. T. Dissociable contributions of phasic dopamine activity to reward and prediction. *Cell Reports* **36** (2021).

43 Ishino, S. *et al.* Dopamine error signal to actively cope with lack of expected reward. *Science Advances* **9**, eade5420 (2023).

44 Grace, A. A. & Bunney, B. S. The control of firing pattern in nigral dopamine neurons: burst firing. *Journal of neuroscience* **4**, 2877-2890 (1984).

45 Ungless, M. A. & Grace, A. A. Are you or aren't you? Challenges associated with physiologically identifying dopamine neurons. *Trends in neurosciences* **35**, 422-430 (2012).

46 Bouton, M. E. Context and behavioral processes in extinction. *Learning & memory* **11**, 485-494 (2004).

47 Lubow, R. E. Latent inhibition. *Psychological bulletin* **79**, 398 (1973).

48 Mogenson, G. J., Wu, M. & Machanda, S. Locomotor activity initiated by microinfusions of picrotoxin into the ventral tegmental area. *Brain research* **161**, 311-319 (1979).

49 Arnt, J. & Scheel-Kruger, J. GABA in the ventral tegmental area: differential regional effects on locomotion, aggression and food intake after microinjection of GABA agonists and antagonists. *Life Sci* **25**, 1351-1360 (1979). https://doi.org/10.1016/0024-3205(79)90402-8

50 Tanner, T. GABA-induced locomotor activity in the rat, after bilateral injection into the ventral tegmental area. *Neuropharmacology* **18**, 441-446 (1979). https://doi.org/10.1016/0028-3908(79)90067-4

51 Barrot, M. *et al.* Braking dopamine systems: a new GABA master structure for mesolimbic and nigrostriatal functions. *Journal of Neuroscience* **32**, 14094-14101 (2012).

52 Zhang, Y. *et al.* Fast and sensitive GCaMP calcium indicators for imaging neural populations. *Nature* **615**, 884-891 (2023). https://doi.org/10.1038/s41586-023-05828-9

53 Zalocusky, K. A. *et al.* Nucleus accumbens D2R cells signal prior outcomes and control risky decision-making. *Nature* **531**, 642-646 (2016).

54 Sasaki, R. *et al.* Balancing risk-return decisions by manipulating the mesofrontal circuits in primates. *Science* **383**, 55-61 (2024).

55 Zachry, J. E. *et al.* D1 and D2 medium spiny neurons in the nucleus accumbens core have distinct and valence-independent roles in learning. *Neuron* (2023).

56 Domingues, A. V. *et al.* Dynamic representation of appetitive and aversive stimuli in nucleus accumbens shell D1- and D2-medium spiny neurons. *bioRxiv*, 2024.2002. 2022.581563 (2024).

57 Shen, W., Flajolet, M., Greengard, P. & Surmeier, D. J. Dichotomous dopaminergic control of striatal synaptic plasticity. *Science* **321**, 848-851 (2008).

58 Lee, S. J. *et al.* Cell-type-specific asynchronous modulation of PKA by dopamine in learning. *Nature* **590**, 451-456 (2021).

59 Coddington, L. T. & Dudman, J. T. The timing of action determines reward prediction signals in identified midbrain dopamine neurons. *Nat Neurosci* **21**, 1563-1573 (2018). https://doi.org/10.1038/s41593-018-0245-7

60 Morice, R. Cognitive inflexibility and pre-frontal dysfunction in schizophrenia and mania. *The British Journal of Psychiatry* **157**, 50-54 (1990).

61 Steuber, E. R. & McGuire, J. F. A systematic review of fear learning, extinction learning, and reversal learning in obsessive-compulsive disorder: implications for treatment. *The Journal of Clinical Psychiatry* **83**, 43190 (2022).

62 Careaga, M. B. L., Girardi, C. E. N. & Suchecki, D. Understanding posttraumatic stress disorder through fear conditioning, extinction and reconsolidation. *Neuroscience & Biobehavioral Reviews* **71**, 48-57 (2016).

63 Torregrossa, M. M. & Taylor, J. R. Learning to forget: manipulating extinction and reconsolidation processes to treat addiction. *Psychopharmacology* **226**, 659-672 (2013).

64 Pekkala, S., Albert, M. L., Spiro III, A. & Erkinjuntti, T. Perseveration in Alzheimer's disease. *Dementia and geriatric cognitive disorders* **25**, 109-114 (2008).

65 Rutledge, R. B. *et al.* Dopaminergic drugs modulate learning rates and perseveration in Parkinson's patients in a dynamic foraging task. *Journal of Neuroscience* **29**, 15104-15114 (2009).

66 González-Rodríguez, P. *et al.* Disruption of mitochondrial complex I induces progressive parkinsonism. *Nature* **599**, 650-656 (2021).

67 Veres, J. M., Nagy, G. A. & Hajos, N. Perisomatic GABAergic synapses of basket cells effectively control principal neuron activity in amygdala networks. *Elife* **6** (2017). https://doi.org/10.7554/eLife.20721

68 Kim, J. *et al.* mGRASP enables mapping mammalian synaptic connectivity with light microscopy. *Nat Methods* **9**, 96-102 (2012). https://doi.org/10.1038/nmeth.1784

69 Bargmann, C. I. How the New Neuroscience Will Advance Medicine. *JAMA* **314**, 221-222 (2015). https://doi.org/10.1001/jama.2015.3298

70 Fisher, S. D. *et al.* Reinforcement determines the timing dependence of corticostriatal synaptic plasticity in vivo. *Nature communications* **8**, 334 (2017).

71 Yagishita, S. *et al.* A critical time window for dopamine actions on the structural plasticity of dendritic spines. *Science* **345**, 1616-1620 (2014).

72 Angela, J. Y. & Dayan, P. Uncertainty, neuromodulation, and attention. *Neuron* **46**, 681-692 (2005).

73 Grossman, C. D., Bari, B. A. & Cohen, J. Y. Serotonin neurons modulate learning rate through uncertainty. *Current Biology* **32**, 586-599. e587 (2022).

74 Pearce, J. M. & Hall, G. A model for Pavlovian learning: variations in the effectiveness of conditioned but not of unconditioned stimuli. *Psychological review* **87**, 532 (1980).

75 Faraji, M., Preuschoff, K. & Gerstner, W. Balancing new against old information: the role of puzzlement surprise in learning. *Neural computation* **30**, 34-83 (2018).

76 Weaver, I. A., Yousefzadeh, S. A. & Tadross, M. R. An open-source head-fixation and implant-protection system for mice. *HardwareX* **13**, e00391 (2023).

77 Siegle, J. H. *et al.* Open Ephys: an open-source, plugin-based platform for multichannel electrophysiology. *Journal of neural engineering* **14**, 045003 (2017).

78 Dzirasa, K., Fuentes, R., Kumar, S., Potes, J. M. & Nicolelis, M. A. Chronic in vivo multi-circuit neurophysiological recordings in mice. *Journal of neuroscience methods* **195**, 36-46 (2011).

79 Yger, P. *et al.* A spike sorting toolbox for up to thousands of electrodes validated with ground truth recordings in vitro and in vivo. *Elife* **7**, e34518 (2018).

80 Ho, J., Tumkaya, T., Aryal, S., Choi, H. & Claridge-Chang, A. Moving beyond P values: data analysis with estimation graphics. *Nature methods* **16**, 565-566 (2019).

81 Berg, S. *et al.* Ilastik: interactive machine learning for (bio) image analysis. *Nature methods* **16**, 1226-1232 (2019).

METHODS

Mice — DAT-IRES-Cre (Jackson Labs 006660) mice were group housed by age and sex (max 5 per cage) in a standard temperature and humidity environment. Mice were housed primarily under a normal 12-hr light/dark cycle and with food and water provided *ad libitum*. Reverse-light-cycle and water-restriction conditions are detailed in Behavioral Experiments. All experiments involving animals were approved by the Duke Institutional Animal Care and Use Committee (IACUC), an AALAC accredited program registered with both the USDA Public Health Service and the NIH Office of Animal Welfare Assurance, and conform to all relevant regulatory standards (Tadross protocols A160-17-06, A113-20-05, A091-23-04).

Recombinant Adeno-associated Viral (rAAV) Vectors — All custom viral vectors were produced by the Duke Viral Vector Core or VectorBuilder. Viruses were kept frozen at -80°C until use, then diluted to the desired titers using sterile hyperosmotic PBS and kept at 4°C for up to 4 weeks.

Acute Brain Slice Preparation and Electrophysiology — DAT-IRES-Cre mice (5 females, 3 males, 8-10 weeks) were anesthetized and stereotaxically injected with 400 nL of either AAV_{rh10}-CAG-DIO-$^{+}HTP_{GPI}$-2A-dTomato-WPRE or AAV_{rh10}-CAG-DIO-$^{dd}HTP_{GPI}$-2A-dTomato-WPRE (2×10^{12} VG/mL, 100nL per site, two tracks with two depths per track: -3.2 mm AP, ±0.5 mm ML, -5.0/-4.5 mm DV) using a custom Narishige injector. After 3-5 weeks for expression, mice were deeply anesthetized with isoflurane and euthanized by decapitation. Coronal brain slices (300 µm) containing VTA were prepared by standard methods using a Vibratome (Leica, VT1200S), in ice-cold high sucrose cutting solution containing (in mM): 220 sucrose, 3 KCl, 1.25 NaH_2PO4, 25 $NaHCO_3$, 12 $MgSO_4$, 10 glucose, and 0.2 $CaCl_2$ bubbled with 95% O_2 and 5% CO_2. The slices were then placed into modified artificial cerebrospinal fluid (aCSF) containing (in mM): 120 NaCl, 3.3 KCl, 1.23 NaH_2PO_4, 1 $MgSO_4$, 2 $CaCl_2$, 25 $NaHCO_3$, and 10 glucose at pH 7.3, previously saturated with 95% O_2 and 5% CO_2. Slices were incubated at 33°C for 40-60 min in the bubbled aCSF solution and then allowed to cool to room temperature (22-24°C) until the recordings were initiated.

Recordings were performed on an Olympus BX51WI microscope, where slices were perfused with bubbled aCSF at 29-30°C with a 2 ml/min flow rate. To isolate $GABA_A$ IPSCs, the aCSF external solution was supplemented with DNQX (20 µM, AMPA antagonist) and AP-V (50 µM, NMDA antagonist). Alternately, to isolate AMPA-mediated EPSCs, aCSF was supplemented with picrotoxin (50 µM, $GABA_AR$ antagonist) and AP-V (50 µM). Finally, NMDA-mediated EPSCs were isolated with picrotoxin (50 µM) and DNQX (20 µM).

For voltage-clamp, the internal solution contained (in mM): 135 CsCl, 2 $MgCl_2$, 0.5 EGTA, 10 HEPES, 4 MgATP, 0.5 NaGTP, 10 Na_2-phosphocreatine, and 4 QX314 (lidocaine N-ethyl bromide), pH 7.3 with CsOH (290 mOsm). For current-clamp, the pipette solution contained (in mM) 130 K-gluconate, 5 KCl, 2 $MgCl_2$, 0.2 EGTA, 10 HEPES, 4 MgATP, 0.5 NaGTP, and 10 phosphocreatine, pH adjusted to 7.3 with KOH (290 mOsm). Internal solutions were used to fill glass recording pipettes (4-6 MΩ). The liquid junction potential was estimated to be 15.9 mV for the normal aCSF solution and was not corrected.

Whole-cell recordings were obtained with Multiclamp 700B and Digidata 1440A, which were controlled by pClamp 10.7 acquisition software (Molecular Devices). Signals were filtered at 10 kHz. A stimulating electrode was placed 60-100 µm from the recorded neuron. Evoked IPSC or EPSC signals were elicited by electrical stimuli of 0.3 ms duration and 150-300 µA (60-70% maximum responses), with a repetition interval of 15 sec. Our inclusion criteria required that cells maintain stable access and holding currents for at least 5 min. In particular, series resistance is monitored using 5–10 mV hyperpolarizing steps interleaved with our stimuli, and cells are discarded if series resistance changed more than ~15% during the experiment. The stored data signals were processed using Clampfit 10.7 (Axon Instruments).

***In Vivo* Electrophysiology Experiments —** Adult DAT-IRES-Cre mice (2 females, 6 males; 12 -16 weeks old) were anesthetized and stereotaxically injected with 400 nL of either AAV_{rh10}-CAG-DIO-$^{+}HTP_{GPI}$-2A-dTomato-WPRE, AAV_{rh10}-CAG-DIO-$^{dd}HTP_{GPI}$-2A-dTomato-WPRE (2×10^{12} VG/mL), AAV_{rh10}-CAG-CreON-W3SL-$^{+}HTP_{GPI}$-IRES-dTomato-Farnesylated, or AAV_{rh10}-CAG-CreON-W3SL-$^{dd}HTP_{GPI}$-IRES-dTomato-Farnesylated (1×10^{12} VG/mL) (100nL per site, two tracks with two depths per track: -3.2mm AP, +- 0.5mm ML, -5.0/-4.5mm DV) with a custom Narishige injector. Mice were then immediately implanted with a single-drive movable micro-bundle electrode array (Innovative Neurophysiology, Inc.; 23µm Tungsten Electrodes, 16/bundle; 0.008” silver ground wire) above the left VTA (-3.2mm AP, -0.5mm ML, -4.0mm DV). The silver ground wire was wrapped securely around two ground screws, one placed in the skull above the cerebellum and one above the right olfactory bulb. A unilateral metal cannula (P1Tech; C315GMN; cut to 13.5mm) was implanted laterally as close as possible to the electrode bundle (-3.2mm AP, -1.3mm ML, -4.0mm DV). The extended length of this cannula

guide places the cannula pedestal above the base of the electrode bundle, allowing for simultaneous attachments of the cannula to an infusion pump and the electrodes to an Intan headstage. Mice were fitted with a plastic head bar adhered to the skull with OptiBond and dental cement, enabling head fixation. Mice were singly or pair housed post-surgery, in a 12-hr light/dark cycle, with food and water provided *ad libitum*. Pair-housed mice were outfitted with head hats that clip to specially designed head bars[76] to prevent cannula or electrode damage from chewing by cage mates.

Electrophysiology recordings and DART infusions were performed at least 3 weeks after surgery to allow for recombinant protein expression. To advance the electrodes to the VTA with minimal damage, the electrode bundle was manually advanced three times: (1) 208 µm at least one week after surgery, (2) another 208 µm one week later, and (3) 104 µm one week later. This placed the electrodes at -4.5 mm DV, at the top of the VTA. After a few days for recovery, electrophysiological recordings were made with an Intan RHD 16-channel headstage with accelerometer (C3335) attached to an Open Ephys Acquisition Board via an Intan RHD 1-ft ultra-thin SPI interface cable (C3211). Data was collected using the Open Ephys GUI[77]. Putative dopamine neurons were identified via their canonical features: tonic firing between 0 and 10Hz, with bursting; biphasic or triphasic waveforms; large amplitudes; and wide waveforms[44,45]. If no putative dopamine neurons were observed online, electrodes were advanced an additional 26-52 µm; this cycle was repeated until multiple channels with putative dopamine neurons were observed, at which point a recording was obtained.

DART ligands, stored as pure-compound aliquots, were freshly thawed on the day of use and dissolved in sterile artificial cerebrospinal fluid (aCSF) containing (in mM): 148 NaCl, 3 KCl, 1.4 $CaCl_2$, 0.8 $MgSO_4$, 0.8 Na_2HPO_4, 0.2 NaH_2PO_4. The final reagent solution contained 10 µM gabazine.7$^{DART.2}$ + 1 µM Alexa647.1$^{DART.2}$. This solution was loaded into an internal cannula designed to project 0.5 - 1.5 mm from the guide cannula, with progressively longer internals used on successive infusions. Mice were head-fixed, the internal cannula inserted, and the Innovative Neurophysiology electrode bundle was connected to the Intan headstage. After obtaining a 15 min baseline recording, we infused 1.5 µL of DART reagent over 15 min (0.1 µL/min; Harvard Apparatus PhD Ultra pump; 5 µL Hamilton syringe), and continued the recording (120 min total). After completion of the recording, electrodes were advanced 26-52 µm. As neurophysiological signals have been shown to remain viable up to 16 months after implantation[78], we obtained multiple recordings from each animal. Mice were given at least two weeks for recovery between recordings, which we have shown is sufficient to allow for complete HTP protein turnover[39].

Spike sorting of the raw data was performed using SpyKING CIRCUS, an open-access software package allowing for semi-manual spike sorting on multichannel extra-cellular recordings[79]. Detection parameters included: spike threshold = 4; N_t (width of templates) = 2 or 3; peaks = positive. Filtering parameters used 250 Hz as the cut off frequency for the Butterworth filter. All other parameters in the configuration file were standard as recommended by the SpyKING CIRCUS documentation. Only templates that matched all features of putative dopamine neurons and exhibited consistent spiking across the whole two-hour recording window were kept for analysis. Semi-manual spike sorting and template extraction was all performed by SCVB for consistency. Custom MATLAB code was used to extract the following metrics:

Tonic: ***FR*** — firing rate (spikes per second)
mISI — median interspike interval (ms)

Pause: ***%PSI*** — % pause-spike intervals (percent of all $ISI > 2 \times mISI$)
PL — pause length, normalized (mean ***PSI*** duration divided by ***mISI***, unitless)

Burst: ***%SFB*** — % spikes fired in bursts (percent of all spikes fired during bursts)
SPB — mean spikes per burst (unitless)

For burst metrics, a burst is defined as a sequence of 3-10 spikes in which the first ISI < 80 ms and subsequent ISI < 160 ms.

Changes in a given metric, m, were analyzed by comparing the 15-min baseline (m_{pre}) to a 15-min sliding window (m_{post}) according to: $\Delta m_{norm} = (m_{post} - m_{pre}) / (m_{post} + m_{pre})$. We then plotted the time course of Δm_{norm} (as a function of the sliding-window time), and analyzed the steady-state Δm_{norm} (1-hr post-gabazine^{DART}) using a two-sided permutation test[80]. Correlations between metrics were analyzed with a Pearson's test.**Behavior Experiments** — Adult DAT-IRES-cre mice (17 females, 20 males; 12 -16 weeks old) were anesthetized and stereotaxically injected with 400 nL of either AAV_{rh10}-CAG-DIO-$^{+}HTP_{GPI}$-2A-dTomato-WPRE or AAV_{rh10}-CAG-DIO-$^{dd}HTP_{GPI}$-2A-dTomato-WPRE (2×10^{12} VG/mL, 100nL per site, two tracks with two depths per track: -3.2 mm AP, ±0.5 mm ML, -5.0/-4.5 mm DV) with a custom Narishige injector. Mice were then immediately

implanted with a bilateral metal cannula above the VTA (P1Tech; C235G-1.0; cut to 4 mm with a 1.0 mm spacing), which was lowered slowly to -3.75mm. Mice were fitted with a plastic head bar adhered to the skull with OptiBond and dental cement, enabling head fixation. Mice were singly or pair housed post-surgery, in a 12-hr reverse light/dark cycle, with food and water provided *ad libitum*. Pair-housed mice were outfitted with head hats that clip to specially designed head bars[76] to prevent cannula damage from chewing by cage mates. Mice were given a minimum of 9 days post-surgery for recovery and acclimation to the reverse light cycle. For the subsequent 3 days, mice were habituated to head-fixation and water restriction. Water was limited to 50-60 µL per gram of the mouse's baseline weight per day, while dry food was provided *ad libitum*. The water restriction goal was 85% starting body weight; additional supplementary water was provided if mice dropped below 77% original body weight or did not pass a daily qualitative health assessment. Only 1 mouse was excluded for issues with water restriction health.

During behavioral sessions, mice were head-fixed (custom 3D printed clamps that fit custom head bars[76]) on a round plastic treadmill (Delvie's Plastics, 8" plexiglass disk covered with silicone rubber) attached to a rotary encoder to collect rotation data (U.S. Digital H5-100-NE-S). Cue tones were played through a Z50 speaker, lick detection was collected with an infrared beam, and sucrose rewards were delivered via a Lee Company solenoid (LHDA1233315H HDI-PTD-Saline-12V-30PSI). A custom MATLAB script controlled the behavioral sessions and data collection via a National Instruments card (NI USB-6351 X Series DAQ). Behavior sessions lasted 1 hr per day for 12 consecutive days and were performed during the dark portion of the mouse's circadian cycle. The order in which each mouse performed the task was pseudo-randomly counterbalanced.

During training sessions (days 1-10), mice were conditioned to associate cue A (2.5 kHz tone, 1.5 sec) with a 5 µL 10% sucrose-water reward. Conditioning trials were randomly interleaved with silent trials (with neither cue nor reward), enabling consistency in the trial-structure and reward-delivery quantities throughout training and testing sessions. On the final day of training (day 10) we replaced 5-6 of the silent trials with probe trials in which an unfamiliar cue B (11 kHz tone, 1.5 sec) was presented but unrewarded. Thereafter, on day 11, we infused 10 µM gabazine.7$^{DART.2}$ + 1 µM Alexa647.1$^{DART.2}$ dissolved in sterile aCSF; 0.6 - 0.8 µL was infused per hemisphere at a rate of 0.1 µL/min (Harvard Apparatus PhD Ultra pump using 5 µL Hamilton syringes). Following a 2 hr rest, mice resumed the original training rules for 15 min. Thereafter the rules changed: cue A was now unrewarded (extinction trials) interleaved with cue B rewarded (conditioning trials). These rules continued on day 12. Throughout the assay, mice completed 200–300 total trials daily (half cue A; half cue B or silent). Licks were allowed during the 1.5 sec tone (anticipatory licks) and the subsequent 2 sec period (retrieval licks). The inter-trial interval (ITI) was random 3 - 13 sec (from the end of the retrieval period to the start of the next cue). Licks occurring during the ITI resulted in a timeout penalty and resetting of the ITI to discourage nonspecific licking. Timeouts were never imposed for licking during a cue or retrieval period (regardless of whether the cue was rewarded or unrewarded).

Anticipatory licking (during the 1.5 sec cue) was our primary learning measure, which we quantify as the fraction of time that the infrared beam was broken during the cue. Our behavioral inclusion criteria required that mice exhibit mean cue A anticipatory licking greater than 0.2 on the 10th training session (this was satisfied by 27/36 mice), and cue B probe-trial anticipatory licking less than 30% of responses to cue A (satisfied by 24/27 mice). The main-text figures include the 24 mice that met our behavioral inclusion criteria (12 ^{dd}HTP, 12 $^{+}$HTP) which all received receiving gabazine.7$^{DART.2}$. The behavioral experimenter was blinded to virus condition in half of the experimental cohorts. Extended Data Fig. 4c contains a total of 25 ^{dd}HTP mice (13 females, 12 males) which include the same 12 ^{dd}HTP mice (receiving gabazine.7$^{DART.2}$) plus an additional 13 ^{dd}HTP mice that also met behavioral inclusion criteria and had received a different infusion (blank.1$^{DART.2}$, diazepam.1$^{DART.2}$, or YM90K.1$^{DART.2}$) at doses shown to have no behavioral ambient drug effects[39]. Following the behavioral session on day 12, all mice were perfused for histological visualization of tracer^{DART} capture. No mice were excluded based on histology.

Fiber Photometry Experiments — Adult DAT-IRES-cre mice (12 females, 12 males; 12 -16 weeks old) were anesthetized and stereotaxically injected with a mixture containing pGP-AAV9-CAG-FLEX-jGCaMP8f-WPRE (5 x 10^{11} VG/mL) and either AAV$_{rh10}$-CAG-DIO-$^{+}$HTP$_{GPI}$-2A-dTomato-WPRE or AAV$_{rh10}$-CAG-DIO-^{dd}HTP$_{GPI}$-2A-dTomato-WPRE (2 × 10^{12} VG/mL) (400 nL total; 100nL per site, two tracks with two depths per track: -3.2 mm AP, ±0.5 mm ML, -5.0/-4.5 mm DV) with a custom Narishige injector. Mice were then immediately implanted with a unilateral mini metal cannula in one hemisphere above the VTA (P1Tech; C315GMN/SPC; cut to 7 mm), at a 5-10 degree angle towards the midline and lowered slowly to -3.75 mm DV. They were also implanted with an optic fiber (Doric Lenses, MFC_400/430-0.66_5mm_MF1.25_FLT) in the second hemisphere, at a 5-6 degree angle towards the midline and lowered slowly to -4.25 mm DV, just dorsal to the VTA. Mice were

fitted with a plastic head bar adhered to the skull with OptiBond and dental cement, enabling head fixation. Mice were singly housed post-surgery, in a 12-hr reverse light/dark cycle, with food and water provided *ad libitum*.

After waiting at least three weeks, mice were started on the multiplexed conditioning/extinction behavior assay as described above, with the additional component of fiber photometry recordings (Tucker-Davis Technologies RZ10X, data collected with TDT Synapse software) collected during every behavioral session. 415 nm (isosbestic) and 465 nm (GCaMP) recordings were obtained. Fibers were bleached in both channels every 1-2 days. Prior to the first testing behavioral session, DART ligands, stored as pure-compound aliquots, were freshly thawed and dissolved in sterile aCSF to 10 μM gabazine.7$^{DART.2}$ + 1 μM Alexa647.1$^{DART.2}$ or 10 μM blank.1$^{DART.2}$ + 1μM Alexa647.1$^{DART.2}$. As infusions could be performed through only a unilateral cannula guide instead of a bilateral one, but bilateral capture was desired, 0.8 nL was infused either 2 or 3 times at a rate of 0.1 μL/min with 1 hour between each infusion (1.6-2.4 μL total; Harvard Apparatus PhD Ultra pump using 5uL Hamilton syringes). This enabled capture equal to that achieved through the bilateral cannulas, without stronger ambient effects from a greater volume infused at once into a single hemisphere. Mice then underwent behavioral testing sessions 2-hr and 24-hr post-infusion, and were perfused immediately after the second behavior testing session to allow histological visualization of jGCaMP8f expression and Alexa647^{DART} capture. Fiber placement at the VTA was visually determined. No mice were excluded based on histology. Mice that did not meet the behavioral criteria described above were excluded (4 mice for cue A anticipatory licking < 0.2 and an additional 2 mice for cue B probe > 30% cue A response). The behavioral experimenter was blinded to virus condition in all of the experimental cohorts.

Fiber photometry signal analysis was performed using custom written MATLAB code. To assess the effects of our manipulation on tonic activity, we computed:

$\Delta(F_0)_{norm} = (F_{0_post} - F_{0_pre})/(F_{0_post} + F_{0_pre})$ where:

- F_{0_pre} is day 8-10 average 465 nm (GCaMP) signal.
- F_{0_post} is day 11-12 average 465 nm (GCaMP) signal.
- F_0 is a double-exponential fit of $F_{0,raw}$ (signal before each cue) vs trial number. This approach provides an estimate of F_0 that accounts for photobleaching while being robust to trial-to-trial noise. A separate fit was performed for each behavioral session, and was visually confirmed to approximate the raw data.

To assess the effects of our manipulation on phasic activity, we computed:
$\Delta F/F_0 = (F - F_0)/F_0$ where F is the instantaneous fluorescence GCaMP intensity. We then defined time intervals as follows: (where t = 0 at the start of the 1.5 sec tone).

- Cue responses were calculated from t = 0.0 to 1.0 sec.
- Reward responses (full width) were calculated from t = 1.5 to 3.0 sec.
- Reward responses (narrow) were calculated from t = 1.75 to 2.25 sec.

Our photometry inclusion criteria required that cue-evoked $\Delta F/F_0 > 1$, averaged over days 6-10 (the stable baseline). This serves as a quality control metric for signal-to-noise. To confirm the appropriateness of this threshold, we performed a regression analysis against our primary metric, the early-pause $\Delta F/F_0$ (first 4 omissions). This regression analysis, which included all mice, confirmed our main finding, which is a strong statistically significant difference between ^{dd}HTP and $^{+}$HTP mice. In addition, the regression analysis confirmed the appropriateness of our inclusion threshold, below which pauses could not be reliably detected in control mice due to low signal quality. All statistical comparisons were between ^{dd}HTP vs $^{+}$HTP mice were determined using two-sided permutation tests[80].

Histology — Mice were deeply anesthetized with isoflurane. For mice with electrodes, we briefly touched each electrode to the positive lead of a 9V battery (1 sec) while the negative lead was grounded to their tongue, thereby creating small lesions to mark electrode positions. Thereafter, all mice were fixed by transcardial perfusion of 15 mL PBS followed by 50 mL ice-cold 4% paraformaldehyde (PFA) in 0.1M PB, pH 7.4. Brains were excised from the skull, further post-fixed in 50mL of 4% PFA at 4°C overnight, and then washed three times with PBS. Brains were embedded in 5% agarose and sliced along the coronal axis at 50 μm (Leica, VT1200S).

For brain sections undergoing tyrosine hydroxylase immunostaining, sections were washed in PBS before a 2 hr incubation in a blocking solution consisting of 5% goat serum, 3% bovine serum albumin, and 0.3% trition-x. Sections were then transferred to a half block solution containing 1:1000 rabbit anti-TH (PelFreez, P40101) overnight at 4˚C with agitation. Sections were then washed in 0.1M PBS containing 0.1% tween before a 4 hr incubation in a half block solution containing 1:1000 goat anti-rabbit 488 (Invitrogen, A11008). Finally, sections were washed in PBS containing tween, then PBS alone prior to mounting on glass slides.

Sections were mounted onto glass slides (VWR 48311-703) and coverslipped with Vectashield mounting medium (Vector Labs, H-1400 or H-1800). Fluorescent images (DAPI, FITC, TRITC, Cy5) were collected at 10X magnification with an Olympus VS200 slide scanner.

Cell counts were obtained using ilastik[81]. Pixel Classification was used to predict cell versus not-cell (background tissue), then Object Classification was used on these pixel predictions to label cells as red (dTomato), green (TH+ or GCaMP), or red+green (both). Object identities were exported and used to calculate the number of cells identified in each label class across all sections from one brain. Separate pixel intensity analysis was performed with a custom MATLAB code. For each coronal section, the VTA was manually segmented in both hemispheres. Background fluorescence was subtracted. Dye capture levels were calculated via a pixel-wise summation over 15 coronal sections. Correlations between pixel intensity and behavior were analyzed with a Pearson's permutation test; trend lines are simple linear regressions, and shading is 95% confidence interval.

Data and Software Availability — All data and software are publicly available.
Protocols: https://doi.org/10.17504/protocols.io.j8nlk8ekdl5r/v1
Software: https://github.com/tadrosslab/VTA_GABA_paper and https://doi.org/10.5281/zenodo.10951255
Datasets:

- **Fig. 1, Extended Data Fig. 1-2:** https://doi.org/10.5281/zenodo.10904059
- **Fig. 2,4, Extended Data Fig. 3, 5:** https://doi.org/10.5281/zenodo.10903566 and https://doi.org/10.5281/zenodo.10908572
- **Fig. 3, Extended Data Fig. 4:** https://doi.org/10.5281/zenodo.10908502

Contact for Reagent and Resource Sharing

Further information and requests for resources and reagents should be directed to and will be fulfilled by the corresponding author Michael R. Tadross, MD, PhD (michael.tadross@duke.edu).

Table S1: Key Resources

REAGENT or RESOURCE	SOURCE	IDENTIFIER
Bacterial and virus strains		
AAV_{rh10}-CAG-DIO-$^{+}HTP_{GPI}$-2A-dTomato-WPRE	Duke Viral Vector Core VectorBuilder	AAV10-X0117A, Lot 200807, 210215, 220331, VB220331
AAV_{rh10}-CAG-DIO-$^{dd}HTP_{GPI}$-2A-dTomato-WPRE	Duke Viral Vector Core VectorBuilder	AAV10-M6360D Lot 200203, 210420, VB220331
AAV_{rh10}-CAG-CreON-W3SL-$^{+}HTP_{GPI}$-IRES-dTomato-Farnesylated	Duke Viral Vector Core VectorBuilder	AAV10-6771A, Lot 220328, VB220209
AAV_{rh10}-CAG-CreON-W3SL-$^{dd}HTP_{GPI}$-IRES-dTomato-Farnesylated	Duke Viral Vector Core VectorBuilder	AAV10-6829B, Lot 220328, VB220209
AAV9-CAG-FLEX-jGCaMP8f-WPRE	Addgene	RRID: 162382
Chemicals, peptides, and recombinant proteins		
gabazine.7$^{DART.2}$	Shields et al 2023	Lot 201109, 220512
Alexa647.1$^{DART.2}$	Shields et al 2023	Lot 200213
blank.1$^{DART.2}$	Shields et al 2023	Lot 210418
YM90K.1$^{DART.2}$	Shields et al 2023	Lot 180712c, 200725
diazepam.1$^{DART.2}$	Shields et al 2023	Lot 210628

Experimental models: Organisms/strains		
B6.SJL-Slc6a3tm1.1(cre)Bkmn/J	Jackson Labs	RRID:IMSR_JAX:006660
Software and algorithms		
MATLAB	MathWorks, Inc	Version 2017b, 2018a, 2020b
OpenEphys	Siegle et al 2017	Version 5.5.3, 6
Spyking Circus	Yger et al 2018	Version 1.0.1
Synapse	Tucker-Davis Technologies	Version 89-51248
Prism	GraphPad	Version 9.5.1, 10.0.3
ilastik	Berg et al 2019	Version 1.4.0.post1

Table S2. Detailed Author Contributions

Team members outlined individual contributions across a standard set of CRediT domains using a live google-sheet, allowing all individuals to discuss and reach consensus. Decisions regarding the delineation between authorship and acknowledgement were decided by the supervising PI, and authorship order was decided by the lead PI with input and discussions with all authors.

Name	ORCID	Contribution
Sasha C.V. Burwell	0000-0003-3553-1365	**Fig. 1, Extended Data Fig. 2:** Conceived, designed, and performed all *in vivo* electrophysiology experiments. Optimized AAV serotype, promoter, surgical procedure, and infusion procedure for dual electrode recording and DART manipulation of VTA dopamine neurons. Performed all spike-sorting analysis to ensure consistent extraction of putative dopamine neurons. Wrote software to extract and analyze sorted cell templates. Performed statistical analysis of spiking data. Performed histology (sample preparation, imaging, cell counting). **Fig. 2, 4, Extended Data Fig. 3, 5:** Conceived, designed, and performed all behavior experiments. Designed and built the reward-learning assay. Wrote software to run the assay and to collect and analyze data. Performed statistical analysis of behavior data. Optimized AAV serotype, promoter, surgical procedure, and infusion procedure for utilizing DART in VTA dopamine neurons. Performed all histology (sample preparation, imaging, image segmentation, and image analysis). **Fig. 3, Extended Data Fig. 4:** Conceived, designed, and performed all fiber photometry experiments. Optimized AAV serotype, promoter, surgical procedure, and infusion procedure for dual GCaMP recording and DART manipulation of VTA dopamine neurons. Wrote software for extracting and calculating dF/F signals. Performed statistical analysis of fiber photometry data. Performed all histology (sample preparation, imaging, and image segmentation). **Extended Data Fig. 1:** Performed virus injection surgeries for slice electrophysiology experiments. Wrote original manuscript draft and prepared original versions of **Fig. 1-4** and **Extended Data Fig. 2-5**. Edited and revised paper and figures. Managed and curated data, including managing deposition into repositories and preparing protocols, and scheduled/planned all experiments. **CRediT**: Conceptualization, Methodology, Software, Validation, Formal Analysis, Investigation, Data Curation, Writing - Original Draft, Writing - Review & Editing, Visualization, Project Administration

Haidun Yan	0000-0003-0916-8865	**Extended Data Fig.1:** Conceived, designed, and performed all electrophysiology experiments in VTA brain slices. Performed GABAR-mediated eIPSCs recording by voltage clamp and manipulated gabazine.7$^{DART.2}$ effects from $^{+}$HTP or ^{dd}HTP virus injected VTA DA neurons. Performed spontaneous and evoked action potentials recording by current-clamp, evaluated which gabazine.7$^{DART.2}$ effects on membrane excitability and endogenous channels from $^{+}$HTP virus injected VTA DA neurons. Performed AMPAR- and NMDAR- mediated eEPSCs recording by voltage clamp and evaluated gabazine.7$^{DART.2}$ effects on excitatory synaptic function in $^{+}$HTP positive VTA DA neurons. Performed evoked action potentials recording in $^{+}$HTP positive VTA DA neurons, tested the effect of bank.1$^{DART.2}$ on the neuronal firings. Wrote original draft of methods for electrophysiology in brain slices, and prepared original version of **Extended Data Fig.1.** Reviewed and provided feedback on manuscript. **CRediT**: Methodology, Validation, Formal Analysis, Investigation, Resources, Writing - Review & Editing, Visualization
Shaun S.X Lim	0000-0001-9312-6275	Designed and cloned different variants of the HTP plasmid constructs, including the optimized variant in the experiment. Assisted with validating HTP expression, and HTL capture and diffusion in dopamine neurons. Separately validated locomotor effects from tethering gabazine.7$^{DART.2}$ on VTA dopamine neurons. Reviewed and provided feedback on manuscript. **CRediT**: Methodology, Validation, Resources, Writing - Review & Editing
Brenda C. Shields	0000-0001-9036-2686	Assisted in original development and characterization of DART reagents. Performed cloning and validation of viral constructs. Prepared all DART and virus aliquots. **CRediT**: Methodology, Validation, Resources, Writing - Review & Editing, Project Administration
Michael R. Tadross	0000-0002-7752-6380	Senior Author & Lead Contact. **CRediT**: Conceptualization, Methodology, Software, Validation, Formal Analysis, Resources, Writing Review & Editing, Visualization, Supervision, Project Administration, Funding Acquisition (Duke Startup. NIH: 1RF1MH117055, 1DP2MH1194025)